Heliyon 10 (2024) e37372

Contents lists available at ScienceDirect

Heliyon

journal homepage: www.cell.com/heliyon

Research article

Ellagic acid improves the symptoms of early-onset Alzheimer's disease: Behavioral and physiological correlates

Abhishek B. Jha [a,*,1], Udit J. Chaube [b], Ashish B. Jha [c]

[a] Department of Pharmacology, Institute of Pharmacy, Nirma University, Ahmedabad, 382481, Gujarat, India
[b] Department of Pharmaceutical Chemistry, Institute of Pharmacy, Nirma University, Ahmedabad, 382481, Gujarat, India
[c] Infosys Ltd, Pune, 411057, Maharashtra, India

ARTICLE INFO

Keywords:
Alzheimer's disease
CREB
Ellagic acid
FAIM-L
Memory

ABSTRACT

Oryza sativa is a globally recognized staple food, rich in essential phyto-phenolic compounds such as γ-Oryzanol (OZ), Ferulic acid (FA), and Ellagic acid (EA). These phytochemicals are known for their potential to beneficially modulate molecular biochemistry. The present investigation aimed to evaluate the neuroprotective and cognitive enhancement effects of *Oryza sativa* phyto-phenolics in a model of early-onset Alzheimer's disease (EOAD) induced by Aβ (1-42) in animals. *In-silico* studies suggested that FA, OZ, and EA have target specificity for Aβ, with EA being further selected based on its potent *in-vitro* Aβ anti-aggregatory effects for exploring neurodegenerative conditions. The *in-vivo* experiments demonstrated that EA exerts therapeutic effects in Aβ-induced EOAD, modulating both biochemical and behavioral outcomes. EA treatment at two dose levels, EA_{70} and EA_{140} (70 μM and 140 μM, respectively, administered i.c.v.), significantly counteracted Aβ aggregation and modulated the Ca^{2+}/Calpain/GSK-3β/CDK5 signaling pathways, exhibiting anti-tauopathy effects. Additionally, EA was shown to exert anti-inflammatory effects by preventing astroglial activation, modulating FAIM-L expression, and protecting against TNF-α-induced apoptotic signals. Moreover, the neuromodulatory effects of EA were attributed to the regulation of CREB levels, Dnm-1 expression, and synaptophysin levels, thereby enhancing LTP and synaptic plasticity. EA also induced beneficial cytological and behavioral changes, improving

Abbreviations: AD, Alzheimer's disease; Aβ, Amyloid beta (1-42); AMO, Aβ monomer; AMD, Amygdala; AMPA, α-amino-3-hydroxy-5-methyl-4-isoxazolepropionic acid; ANOVA, Analysis of variance; APP, Amyloid precursor protein; BBB, Blood brain barrier; CA, Cornus ammonis; cDNA, Complementary DNA; CREB, Cyclic AMP response element binding protein; CS, Conditional stimuli; DAB, 3, 3′- diaminobenzidine; DG, Dentate gyrus; DGEC, Dentate gyrus ectal limb; DGEN, Dentate gyrus endal limb; Dnm-1, Dynamin-1; DMSO, Dimethyl sulfoxide; DONO, Donepezil; EA, Ellagic acid; EGTA, Ethylene glycol-bis(β-aminoethyl ether)-N,N,N′,N'-tetraacetic acid; ELISA, Enzyme linked immunosorbent assay; ERC, Entorhinal cortex; EOAD, Early onset Alzheimer's Disease; FA, Ferulic acid; FAD, Familial Alzheimer's Disease; FAIM-L, Long form of Fas apoptotic inhibitory molecule; GFAP, Glial fibrillary acidic protein; GSK, Glycogen synthase kinase; HRP, Horseradish peroxidase; IDE, Insulin-degrading enzyme; LRP, Low-Density Lipoprotein Receptor-Related Protein 1; LTP, Long term potentiation; MMP, Matrix metalloproteinase; MWM, Morris water maze; NMDA, N-methyl-D-aspartate; OZ, γ-Oryzanol; PCR, Polymerase chain reaction; PFC, Prefrontal cortex; PBS, Phosphate buffer saline; p-Tau, Phosphorylated tau; PMSF, Phenylmethylsulfonyl fluoride; RAGES, Receptor for advanced glycation end products; RNA, Ribonucleic Acid; RT-PCR, Reverse transcription PCR; RyR, Ryanodine receptors; SAD, Sporadic Alzheimer's Disease; SCARB, Scavenger receptor class B type 1; SGZ, Subgranular zone; SH, Sham operated group; ThT, Thioflavin T; TNF, Tumor necrosis factor; UCS, Unconditional stimuli; VDCC, Voltage-dependent calcium channels.

* Corresponding author.
E-mail address: abhishek-jha@uiowa.edu (A.B. Jha).
[1] Current address: Department of Internal Medicine, Roy J. and Lucille A. Carver College of Medicine, University of IOWA, Iowa City, IA 52242, United States of America.

https://doi.org/10.1016/j.heliyon.2024.e37372
Received 25 June 2024; Received in revised form 27 August 2024; Accepted 2 September 2024
Available online 7 September 2024

both long-term and short-term spatial memory as well as associative learning behavior in the animal model, which underscores its cognitive enhancement properties.

1. Introduction

Alzheimer's disease (AD) is a global threat, associated with progressive and continuous retardation in cognitive function which involves loss of the functional neurons (i.e. cholinergic neurons) and associated communicating synapses along with the existence of specific pathological markers i.e. senile plaques, neuropil threads, and neurofibrillary tangles incorporated with phosphorylated tau [1]. The aggravators involve a modified lifestyle, deceitful social habits, anomalous peripheral or central metabolism, and mutagenesis in functional genes. Moreover, chemical exposure and psycho-physiological stress are also major risk factors for AD-associated dementia. AD abnormalities are accompanied by intrusion in the cerebral downstream secondary messenger system associated with the regulation of synaptic plasticity, neuronal firing, and neural architecture [2] along with the accumulation of detrimental neuronal byproducts i.e. extracellular amyloid beta (Aβ) and intracellular neurofibrillary tangles (NFT) [3]. AD is accountable for about 50 % of age-associated pathology of dementia and its outbreak is raised from 1 to 5% in people aged above 65 years, and up to 20–25 % in the 80-year-old population [4].

Ferulic acid (FA), an aromatic phenolic phytoconstituent of *Oryza sativa* is the most potential molecule that exists in an esterified form i.e. γ-Oryzanol (OZ) by establishing an ester bond with cyclopentanperihydrophenanthrene [5]. Fundamentally, OZ is constituted of cycloartenyl ferulate, campestryl ferulate, 24-methylene cycloartanyl ferulate, and sitosteryl ferulate [6]. OZ is reported for anti-oxidative, anti-AchE [7], anti-inflammatory [8], immunomodulatory [9], anti-atherosclerotic, anticancer [10], and anti-diabetic [11] properties. Scientific evidence based on recent research by different investigators has revealed lucrative properties of FA against cognitive inadequacies in Aβ (1-40), scopolamine, and central neurotoxin i.e. ethylcholine mustard aziridinium ion (AF64A) treated experimental animals at a dose of 100 mg/kg [12]. Chemically ellagic acid (EA) is a phytopolyphenolic lactone ($C_{14}H_6O_8$) [13] and has been known to alter profuse signaling inside cells to pauperize progression of diverse neurodegenerative abnormalities. Its neuroprotective effectiveness is attributable to its ROS scavenging, iron chelating properties, positive regulation of energetics of mitochondrial respiratory complex, and abundant modulation of neuronal molecular signaling pathways [14].

Present work reports screening of the most potent phytoconstituent from OZ, FA, and EA after *in-silico* docking and *in-vitro* Aβ (1-42) (Aβ) antiaggregatory assay followed by *in vivo* investigation of EA in Aβ induced amyloidopathy in experimental rodents.

2. Materials and methods

2.1. Chemicals

EA was procured as the gratis sample from Sami Labs Ltd, India, OZ was procured from TCI Chemicals (India) Pvt. Ltd., and DONO was provided by Troikaa Pharmaceuticals Limited, Ahmedabad, India. Aβ (1-42) (A9810–0.1 mg) and Rat Aβ (1-42) (SCP0038-1 MG) were procured from Sigma, USA. 1, 1, 1, 3, 3, 3-hexafluro-2-propanol (HFIP) was purchased from CDH. DMSO was procured from Himedia Labs, Mumbai, India. Prime script first strand cDNA synthesis kit, triazol (RNAiso Plus), and PCR master mix (Clontech) were procured from Takara, USA. ELISA kits for Aβ, p-Tau, CREB, and calpain-1 as well as Ca^{2+} assay kits were purchased from Elabscience, USA. TNF-α ELISA kit was procured from Krishgen, USA.

2.2. Molecular docking

Since no inbuilt ligand was available in RCSB-PDB and neither the information regarding the active site for Aβ was available, interactions study with the test molecules was carried out using the psim findcav method in SYBYL X of Tripos Associates, St. Louis, MO, USA and the ProtoMol was created followed by energy minimization. Previously this method has been reported for successful identification of ligand binding sites in targeted proteins [15]. After the creation of ProtoMol the prepared protein and the energy-minimized investigational molecules were saved in .PDB and .SDF format respectively and uploaded to Pose View Center for Bioinformatics: Universität Hamburg [16] to get 2-dimensional images of protein-ligand interaction and the hydrogen bond, π-π, and hydrophobic interactions between amino acid and investigational molecules were analyzed. The crash score and polar score were taken under consideration to evaluate the degree of interaction concerning the appropriateness of penetration in the binding cavity as well as hydrogen-bond interaction. The higher hydrogen-bond interaction was more emphasized to assess the superior ligand likeliness of the test molecule.

2.3. In vitro Aβ antiaggregatory assay

Aβ was dissolved in 888 μL 100 % HFIP to get 25 μM of effective concentration and sonicated for 10 min. Then the solution was allowed to be kept at RT for 1 h. With a gentle flush of nitrogen stream, the HFIP was evaporated to obtain a thin transparent film of Aβ. Until utilization the prepared vial was stored in dry ice. At the time of use, the dried film was reconstituted with 10 % DMSO in 7.4 pH PBS. In Black corning 96 well plate, 9 μL Aβ (Control) and Aβ with 5 μL of the test molecules i.e. OZ, FA, EA, and DONO were dispensed in the respective wells at different concentrations and incubated at 37 °C in the incubator for 48 h. After completion of incubation, 200

μL of 5 μM ThT in glycine buffer (pH 8.0) was administered in each of the wells. After stabilization of ThT, the fluorescent intensity was measured at 446 nm excitation and 490 emission wavelengths through a fluorescent plate reader (TECAN). The % reduction in Aβ aggregation was calculated from the following formula [17–20] and the images were taken at 250× magnification under the fluorescent microscope.

$$\%\ A\beta\ (1-42)\ \text{antiaggregatory activity} = \frac{(\textit{Intensity of control} - \textit{Intensity of blank}) - (\textit{Intensity of test} - \textit{Intensity of blank})}{(\textit{Intensity of control} - \textit{Intensity of Blank})}\ \text{X}\ 100\%$$

2.4. Animals

6–9 months old male Wistar rats weighing 300–470 g were taken from the animal house facility of the Institute of Pharmacy, Nirma University. The experimental protocol was approved by the Institutional Animal Ethics Committee of the Institute of Pharmacy, Nirma University. Project No. IP/PCOL/PHD/21/013. The animals were accustomed to a 12-h day/night cycle at 22 ± 2° C and were allowed free access to food pallets (Pranav Agro Foods Pvt. Ltd., Vadodara) and water.

2.5. Animal grouping and treatment protocols

The animals utilized in the protocol were acclimatized for 7 days in laboratory conditions and trained 5 days before the experiment for evaluation of behavior paradigms associated with cued/delayed avoidance test. A priori power analysis was conducted using G*Power software to determine the appropriate sample size for the study. A total sample size of 84 animals, divided into four groups (n = 21 per group) namely, Sham control (SH), Aβ + Vehicle (AB), Aβ + EA_{70} (EA_{70}), and Aβ + EA_{140} (EA_{140}). The analysis assumed a large effect size (f = 0.8), an alpha error probability of 0.05, and one covariate. The analysis indicated a noncentrality parameter (λ) of 53.76, a critical F-value of 2.72, denominator degrees of freedom of 78, and a power (1-β error probability) of 0.9999976. These results suggest that the study is highly powered to detect significant differences between the groups. Neurodegeneration was induced in all the groups except the SH group by 10 μL rat Aβ monomer (AMO) (10 μL of 1 μg/μL (221.5 μM), i.c.v.).

2.5.1. Surgical method

With quite modifications in the published methods, the surgical process was performed. Animals were anesthetized by ketamine (100 mg/kg, i.m.) and diazepam (5 mg/kg, i.p.) [21]. With the help of a dental drill (Marathon), a bur hole was made in the skull at the coordinate of −1.0 mm A/P, 1.5 mm M/L, and 3.5 mm D/V from the bregma. A clean sterilized guiding cannula was mounted and lowered slowly at the specified ventral coordinate. The anchor screw was inserted ipsilateral and contralateral to the burr hole. A thick layer of dental cement (Zinc F+, Zinc phosphate cement) was applied to cover the screw to secure the guiding cannula at the place. The incision was disinfected with povidone-iodine ointment (10 %). Before the attainment of consciousness, the animals were housed individually in different cages. The guiding cannula was sealed by a dummy cannula.

2.5.2. Aβ monomer (AMO) preparation

AMO was formulated by the formerly described method [22]. With slight modification, the Rat Aβ solution was prepared in 1 mL HFIP. After 10 min of sonication in ice-cold conditions, the solution was divided into 20 aliquots with 50 μL each. After 15 min of air-drying on an ice bath, the HFIP was removed by gentle nitrogen flush. The microcentrifuge tubes containing thin film were kept at −30° C for further usage. Before initiation of the surgical procedure monomer peptide was reconstituted with 10 μL DMSO followed by sonication for 10 min and diluted by 40 μL of 10 mM 7.4 pH PBS to get a final concentration of 221.5 μM (1 μg/μL). The resultant solution was sonicated again for 1 min and used immediately.

2.5.3. AMO and drug administration

AMO (10 μL, 1 μg/μL) was administered in all the groups except the SH group through an insertion cannula at the flow rate of 1 μL/min. In the EA_{70} and EA_{140} groups, 10 μL EA (70 μM and 140 μM; prepared in 10 % DMSO in 7.4 pH PBS) were administered i.c.v. once 180 min before administration of AMO at the flow rate 1 μL/min. Animals of the AB group were treated with 10 % DMSO in 7.4 pH PBS. The dose of ellagic acid (EA) was selected based on an *in vitro* Aβ oligomer inhibition test and safety assessment by resazurin assay.

2.6. Behavioral assessment

At the end of the study behavioral assessment was carried out by water maze to determine spatial working and reference memory and a cued/delayed conditional avoidance test was carried out using Cook's pole climbing apparatus to test the associative memory.

2.6.1. Morris water maze task (MWM)

Three start locations were set in three different quadrants of the water maze and labeled as B, C, and D. In the A quadrant the escape platform was placed. To each of the animals, 1 min of a single trial was given from every starting point. One minute of resting period was given to each animal between every trial from different starting points. Those animals that took more than 1 min to reach the escape platform were guided to the platform and allowed to stand on the platform for 1 min and their escape latency was recorded as 60s. The study was conducted for 5 days and on the 6th day a probe trial was performed to evaluate spatial reference memory and

learning behavior. The swimming pattern and speed of swimming were recorded through Intex Webcam with the help of video tracking software [23].

2.6.2. Cued/delayed conditioned avoidance behavior test for learning and memory (CCA)

Animals were acclimatized for 7 days before baseline evaluation of the Cued/delayed avoidance behavior test in animals. After acclimatization, for the next 5 consecutive days, animals were trained for cued/delayed avoidance tasks to assess the learning ability of animals against unconditional stimuli (shock). For this on the first day of training animals were exposed to experimental apparatus (i.e. Cook's Pole climbing apparatus) for 2 min. After 25 s of conditional stimuli (sound) 20–25 shocks (200-V 2 mA 50 Hz) were given for 1 s at the interval of 2 s. The lag phase between conditional and unconditional stimuli was reduced gradually as described in the training scheme (Fig. 1). The study was terminated on the fifth day. The average latency for pole climbing and the percentage of cued/delayed conditional avoidance were calculated. After completing the treatment protocol, the ability of trained animals to differentiate between conditional and unconditional responses was assessed. Additionally, to confirm that the increase in latency was due to the toxic effects of Aβ, the test was performed on the third day, following a one-day rest phase.

2.7. Tissue homogenate preparation

The brain was removed from each animal (n = 12) after reperfusion with 7.4 pH PBS on the 30th day. The hippocampus, amygdala (AMD), and prefrontal cortex (PFC) were isolated from each rat brain as per the reported method [24] on ice chilled metal plate. Lysis buffer (0.1 M Tris, 150 mM NaCl, 1 % Triton-X, 0.5 % sodium deoxycholate, 1 mM EGTA was stored at 2–4 °C until use and just before preparation of homogenate protease inhibitor cocktail, phosphatase inhibitor cocktail, and 1 mM PMSF were added freshly in 100 mL lysis buffer. The tissue homogenates of isolated regions of each brain (n = 6) were prepared in a 1:10 ratio of tissue: Lysis buffer in an ice bath. The homogenate was stored immediately at −80 °C until use. During evaluation, the homogenates were thawed at RT and centrifuged at 10,000 RPM for 10 min at 4 °C. The clear supernatants were used to quantify p-tau, Aβ, CREB, calpain-1, and TNF-α. The remaining brain sections were homogenized in ice-cold deionized water to estimate the Ca^{2+} level in brain tissue. For this tissue and deionized water were mixed in a 1: 9 ratio and homogenized in an ice water bath and centrifuged at 2500 RPM for 10 min and supernatant was taken for calcium level assessment.

2.8. Biochemical parameters

2.8.1. Blood collection

Blood samples were obtained from each animal via retro-orbital puncture and were left undisturbed for 30 min to allow clot formation. The serum was separated at 4 °C at 7500 RPM for 7 min. The serum was utilized to measure serum Aβ, p-tau, and TNF-α levels.

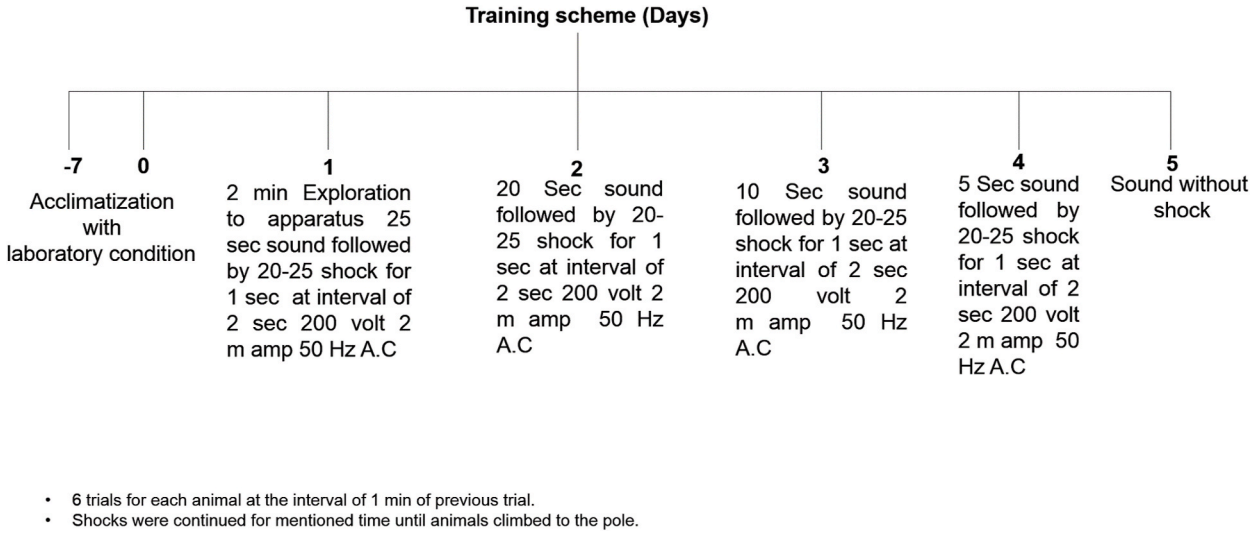

Fig. 1. Acclimatization and training scheme for conditional fear avoidance prior to induction. This figure illustrates the acclimatization process, and the training scheme used to condition the animals for the conditional fear avoidance task before the induction phase. The protocol includes a period of environmental acclimatization, followed by a series of training sessions designed to establish a learned fear response to conditional stimuli. The schematic outlines the timeline and key steps in preparing the animals for the experimental procedures, ensuring consistency and effectiveness in the behavioral conditioning required for the study.

2.8.2. ELISA

100 μL of standards Aβ, p-tau, CREB, Calpain-1, and TNF-α were used to prepare the calibration curve (Concentrations were taken as per the manufacturer's manual of ELISA). Homogenates' supernatant and serum were added to the rat anti-Aβ antibody pre-coated 96 wells and allowed to be incubated for 90 min at RT. The contents from each well were decanted by gentle tapping on absorbing blot paper but not washed by washing buffer. 100 μL of biotinylated detection antibody was dispensed to each well and allowed to incubate at RT for 60 min. Each well was washed 3 times at intervals of 1 min of soak time by 300 μL 1× washing buffer. 100 μL streptavidin-coated HRP conjugate was added and incubated for 30 min at RT. Each well was washed 5 times with 1 × washing buffer at the interval of 1 min soak time. The plate was incubated with 90 μL TMB for 15 min at RT in dark conditions. At the end 50 μL stop solution was added immediately and the plate was read at 450 nm in Readwell touch ELISA plate reader. The concentration of Aβ, p-tau, and TNF-α in brain tissue homogenates was reported as pg/mg protein. While CREB and Calpain-1 were reported as pmol/mg protein and ng/mg protein respectively. Serum levels of Aβ, p-tau, and TNF-α were reported as pg/mL.

2.8.3. Brain calcium

Brain calcium (Ca^{2+}) level was estimated by the colorimetric method through a calcium assay kit. For this 2.5 μmol/mL calcium standard solution was diluted to 1 μmol/mL by deionized water. The detection solution was prepared by mixing MTB reagent, alkaline solution, and protein clarifier in a 10:20:1 ratio. Immediately 10 μL deionized water, 10 μL standard, and 10 μL supernatant were dispensed in the respective wells and mixed with 250 μL of detection solution then incubated for 5 min. The absorbance was measured at 630 nm in a well plate reader. The Ca^{2+} level was estimated from the following formula. The level was represented as μmol/mg protein.

$$\text{Calcium level} = \frac{(\textbf{\textit{Absorbance of sample}} - \textbf{\textit{Absorbance of blank}})}{(\textbf{\textit{Absorbance of standard}} - \textbf{\textit{Absorbance of Blank}})} \text{ x Concentration of standard} \div \text{Protein concentration}$$

2.9. Gene expression study

Gene expression studies for FAIM-L, Dnm-1, GSK-3β, and CDK5 were carried out from rat brain hippocampus and PFC (n = 3). Primers with the sequence provided in Table 1 were designed with the help of the NCBI primer designing tool. The RNA isolation was carried out using triazole (RNAisoplus) and subsequent cDNA was synthesized by prime script 1st strand cDNA synthesis kit, Takara. The genes were amplified at the Tm given in Table 1. The extent of amplification for each amplicon was analyzed through a gel documentation system (Biotop, florshot EVO, Shanghai Bio-Tech Co. LTD) after gel electrophoresis. The intensity of bands was quantified using ImageJ software.

2.10. Fixation of brain sections

The brain was fixed using whole-body perfusion while the rats were anesthetized with 100 mg/kg ketamine and 5 mg/kg diazepam. The brain was then isolated, post-fixed, and stored according to the previously described method [25].

2.11. Histopathological changes

Histopathological analyses were conducted following a previously published method [26] with reference to the Brain Explorer-2 software, version 2.3.5, a digital rat brain atlas. The reperfused rat brains were fixed in Bodian's fixative for 48 h, sectioned into 5 mm thick coronal slices, and embedded in paraffin wax. Thin coronal sections, 5 μm in thickness, were then obtained using a microtome. Hematoxylin-eosin (HE) staining was performed according to the reported protocol [27]. The anatomical structures of the hippocampus proper, including the CA1, CA2, and CA3 regions, and the DG, as well as the interconnecting areas such as the ERC and PFC, were analyzed under a light microscope (Olympus America Inc.) at 250× magnification. The AMD was examined at 400× magnification.

Table 1
Gene specific primers for RT-PCR and Tm.

Genes	Primers	Tm
GAPDH	F 5′- ATGTTCGTCATGGGTGTGAACCA-3′	62.64
	R 5′- TGGCAGGTTTTTCTAGACGGCAG-3′	63.23
FAIM-L	F 5′-TAAGAAGAGAGTGGATGTTCAAGC-3′	58.52
	R 5′- GTAACAGTCGTGGTTCCCCA-3′	59.61
Dnm-1	F 5′- ACTGACCAACCACATCCGGGA	63.48
	R 5′-AAGCGTTCGTGGAAGATCCGG-3′	63.01
GSK-3β	F 5′- GGAGAACTGGTGGCCATCAAGAAAG -3′	63.79
	R5′- GCTTTGCACTTCCAAAGTCGCAG-3′	63.44
CDK5	F 5′- AGCCGTAACGTGCTGCACAG-3′	63.64
	R 5′- AGCTGGTCATCCACATCATTGCC -3′	63.38

2.12. Silver stain

The silver staining was performed by Bielschowsky's method [28]. The deparaffinized brain sections (n = 3) from each group were hydrated with double distilled water, placed on slides, and stained with 2 % silver nitrate under a dark chamber for 2 days. Next, the sections were rinsed with double distilled water several times and placed in the chamber having ammoniacal silver nitrate solution for 20 min. The sections were again rinsed and treated with 0.2 % gold chloride solution for 1 h. The sections were washed to remove excess stain and processed with 5 % sodium thiosulfate for 1 min. Sections were washed again, dehydrated by xylene, and fixed on the slide with DPX: xylene mounting solution. The slides were studied for silver-stained plaques and NFT in similar regions of all brain sections i.e. CA1, CA2, CA3, DG, ERC, and PFC at 250× and AMD at 400× magnification under phase contrast microscope (Olympus America Inc.).

2.13. Immunohistochemistry

The deparaffinized brain sections were gently cleaned under running tap water, autoclaved at 121 °C for 20 min, and soaked in distilled water for 1.5 h. After treatment with 3 % H_2O_2 solution, the sections were again washed with PBS. The thin coronal sections were allowed to react with the primary antibody of GFAP and synaptophysin for 35 min at RT. After the removal of unbound antibodies by washing with PBS, the HRP-conjugated secondary detection antibodies were added and allowed to react for 30 min at RT. The sections were again washed with PBS to remove residual secondary antibody. 3, 3′- diaminobenzidine (DAB), the HRP substrate was added to develop color. The residual unreacted DAB was removed by washing with running water. Nucleus were stained by counterstaining with hematoxylin. The residual stain was removed by washing under running warm water and dehydrated with blotting paper. The stained sections were mounted permanently on the slide with the DPX: xylene mixture. The slides were studied for the immunoreactivity of GFAP (100×) and synaptophysin in similar regions of all brain sections i.e. CA1, CA2, CA3, DG, ERC, and PFC) at 250 × and AMD at 400× (for both GFAP and synaptophysin) magnification under phase contrast microscope (Olympus America Inc.). The images were prepared for analysis by Digimizer version 5t.4.2. Mean GFAP count and mean synaptophysin count were performed by Image J software version 1.46r.

2.14. Statistical analysis

Statistical analyses and graph generation were performed using GraphPad Prism software, version 10 (GraphPad Software, San Diego, CA, USA). Data are presented as Mean ± SEM, and a p-value of <0.05 was considered statistically significant. To evaluate the interaction between treatment and brain regions in ELISA, gene expression, and immunohistochemistry analyses, a two-way ANOVA was initially conducted. Differences among all groups (SH, AB, EA70, and EA140) were then analyzed using one-way ANOVA, followed by Dunnett's multiple comparison test.

For behavioral assessments, including the Morris Water Maze (MWM) test (acquisition trials) parameters (escape latency, swimming velocity, and total distance) and the Cued/Delayed Conditional Avoidance (CCA) test (training) parameters (% cued/delayed conditional avoidance and average latency for pole climbing), treatment × day interactions were evaluated using repeated measures (RM) two-way ANOVA. Significant differences among the groups, including outcomes of the MWM probe test and CCA retrieval evaluations, were further analyzed using one-way ANOVA followed by Dunnett's multiple comparison test.

3. Results

3.1. Interaction of drugs with Aβ

Molecular docking revealed different binding interactions of investigational compounds with Aβ at the generated protomol at the chain–A in its α-helical form. The amino acid interactions of Aβ with DONO, FA, OZ, and EA components are shown in Fig. 2(A–F).

DONO (crash score: −1.0611, polar score: 1.0483) exhibited hydrogen bond interaction with His13, hydrophobic interaction with Phe20, Val24, Ile31, and Leu34 as well as π-cation interaction with NH^{3+} of Lys16. 4-OH, group of FA (crash score: −0.3819, polar score: 1.1933) forms hydrogen bond interaction with Leu17. Furthermore, its benzene ring forms a hydrophobic interaction with Leu17. The carbonyl group of ferulate ester in 24-methylene cycloartanyl ferulate (crash score: −1.2011, polar score: 1.3717) forms classical hydrogen bonding with NH^{3+} of Lys16 whereas the rest of the sterolic counterpart revealed hydrophobic interaction with Met35. The campestryl ferulate (crash sore: −1.1674, polar score: 0.0170) revealed a similar classical hydrogen bond as well as hydrophobic interaction as revealed by 24-methylene cycloartanyl ferulate with additional Phe20 hydrophobic interaction. Cycloartenyl ferulate (crash sore: −0.7834, polar score: 0.0000) revealed neither hydrogen bond nor hydrophobic interactions with Aβ (Fig. 2 G). Sitosteryl ferulate (crash score: −2.1056, polar score: 1.3297) exhibited hydrogen bond interaction with Lys16 through the oxygen of ferulate which takes part in esterification with sterol. The remaining sterolic portions revealed hydrophobic interactions with Leu17, Lys28, and Phe20. EA (crash score: −0.9662, polar score: 2.6946) showed π-π staking interaction with Phe20, hydrogen bond interaction with Leu17 and Lys16. Interestingly, EA revealed two hydrogen bond interactions: one with the NH_3^+ group and another with the carbonyl group (C=O) of Lys16, through its carbonyl (C=O) and hydroxyl (-OH) groups, respectively, suggesting potent H-bonding of EA at the Aβ interaction site.

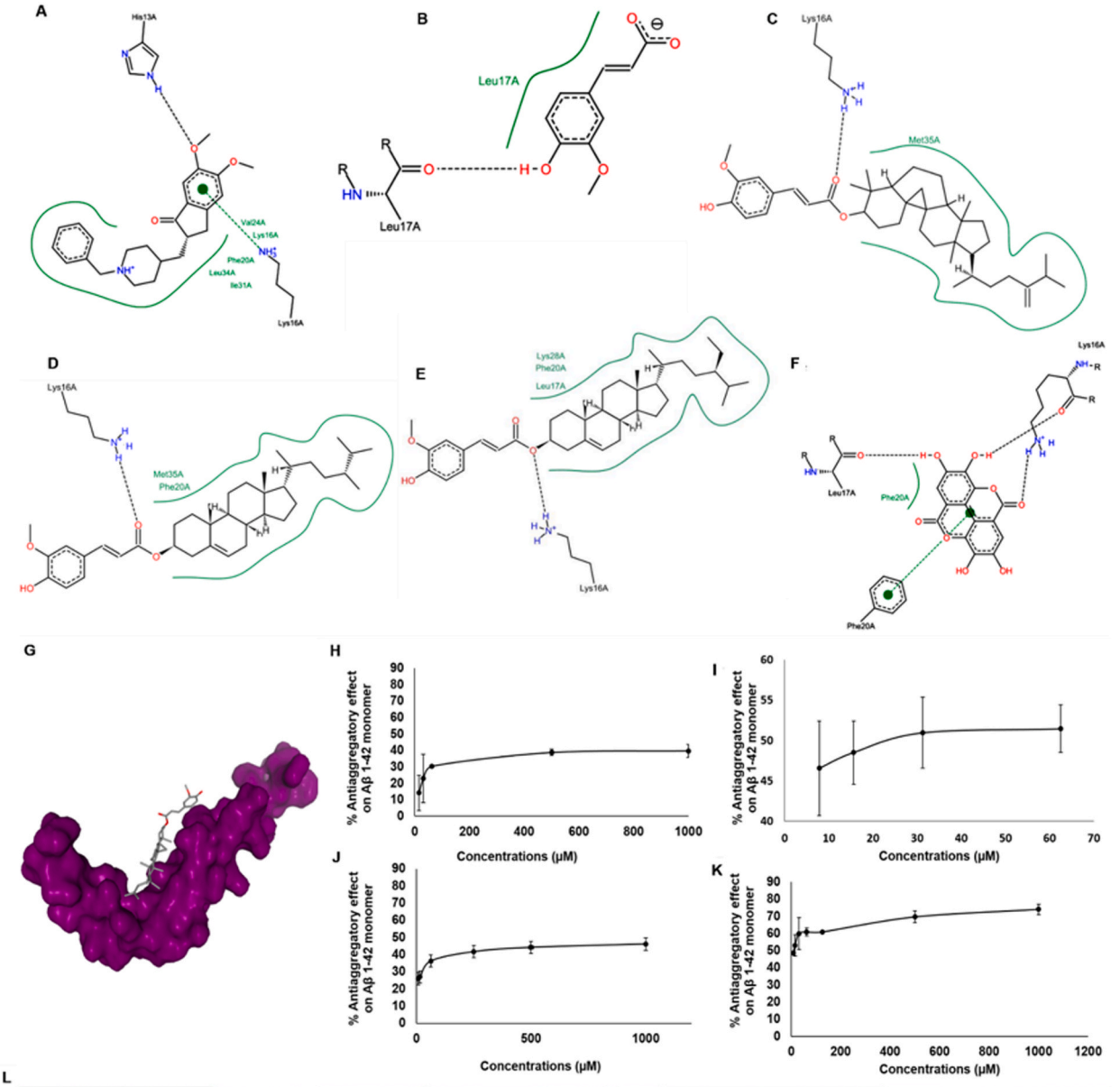

(caption on next page)

Fig. 2. Docking interactions of A) DONO; B) FA; C) 24-methylene cycloartanyl ferulate; D) Campestryl ferulate; E) Sitosteryl ferulate, and F) EA with Aβ. Black dashed lines exhibit hydrogen bonds. Green solid lines represent hydrophobic interactions, and green dashed lines show π-π and π-cation interactions. *No hydrogen-bond or other interactions were shown by Cycloartenyl ferulate; hence, no 2-D pose view image was created. G) 3-D graphical representation of Cycloartenyl ferulate position revealing no interaction with Aβ. The graph of % Antiaggregatory effect on % Aβ Vs Concentrations (μM). % Aβ (1-42) anti-aggregatory effects of H) DONO; I) FA; J) OZ, and K) EA. All data are represented as Mean ± SEM (n = 6). L) Effects of investigational molecules on Aβ aggregation pattern at 62.5 and 500 μM. Magnification: 250×, scale bar: 10 μm.

3.2. *Aβ anti-aggregatory assay*

To validate the in silico docking results, the *in vitro* Aβ anti-aggregatory potentials of DONO, FA, OZ, and EA were evaluated. Several phenolic acids have been reported to exhibit anti-amyloidogenic effects [29]. Our investigation demonstrates the percentage of Aβ anti-aggregatory effects of DONO ($IC_{50} > 1000$ μM), FA ($IC_{50} > 1000$ μM), OZ ($IC_{50} = 30.81 \pm 3.64$ μM), and EA ($IC_{50} = 8.01 \pm 0.5$ μM) as shown in Fig. 2H–K, respectively, against 25 μM of Aβ (Fig. 2 L). A dose-dependent increase in the percentage of Aβ anti-aggregatory effect was observed with all the compounds.

3.3. *Effects of EA on AB-induced plaque formation and tau phosphorylation*

AD reveals the existence of various pathological hallmarks i.e. extra neuronal oligomeric plaque due to Aβ deposition, intra neuronal NFTs due to tau hyperphosphorylation, and substantially active glial cells involved in gliosis inside the cerebral realm [30]. The current study signified the existence of all these classical biochemical alterations in rat brains more precisely in the hippocampus, PFC, and AMD in association with the activation of several upstream and downstream signals after i.c.v. AB administration which contributes to the progression of AD pathogenesis.

3.3.1. *Aβ level*

A significant elevation in Aβ levels was observed in the brain, specifically in the hippocampus ($DF = 3$, $F(3, 20) = 8.509$, $p = 0.0011$), PFC ($DF = 3$, $F(3, 20) = 11.49$, $p = 0.0003$), and AMD ($DF = 3$, $F(3, 20) = 39.00$, $p < 0.0001$), as well as in the serum ($DF = 3$, $F(3, 20) = 22.29$, $p < 0.0001$) of the AB group animals compared to the SH group. The EA_{70} group showed a significant decline in Aβ levels in the brain (hippocampus: $p = 0.0103$; PFC: $p = 0.0035$; AMD: $p < 0.0001$) as well as in serum ($DF = 3$, $F(3, 20) = 22.29$, $p = 0.0001$). EA_{140} treatment group also showed significantly reduced Aβ levels in the brain (hippocampus: $p = 0.0028$; PFC: $p = 0.0005$; AMD: $p < 0.0001$) as well as in serum ($p < 0.0001$) compared to the AB group (Fig. 3 B).

3.3.2. *Calcium/Calpain-1 levels*

Animals from the AB group showed a significant elevation in Ca^{2+} levels (hippocampus: $DF = 3$, $F(3, 20) = 10$, $p = 0.0032$; AMD: $DF = 3$, $F(3, 20) = 3.628$, $p = 0.0215$) as well as in calpain-1 levels (hippocampus: $DF = 3$, $F(3, 20) = 8.312$, $p = 0.0006$; PFC: $DF = 3$, $F(3, 20) = 4.761$, $p = 0.0127$; AMD: $DF = 3$, $F(3, 20) = 28.07$, $p < 0.0001$) when compared with the SH group. EA_{70} treatment significantly reduced calpain-1 levels in the PFC ($p = 0.0069$) and AMD ($p < 0.0001$), while EA_{140} treatment revealed significant reductions in calpain-1 levels in the PFC ($p = 0.0110$) and AMD ($p = 0.0051$). Changes in the hippocampus were statistically insignificant at both dosages compared to the AB group (EA_{70}: $p = 0.9040$; EA_{140}: $p = 0.1177$). A significant reduction in cerebral Ca^{2+} levels was observed in the hippocampus (EA70: $p = 0.0009$; EA140: $p = 0.0001$) and PFC ($DF = 3$, $F(3, 20) = 5.151$; EA_{70}: $p = 0.0069$; EA_{140}: $p = 0.0089$) at both concentrations. In the amygdala (AMD), only the EA_{70} group showed a significant reduction in Ca^{2+} levels compared to the AB group ($p = 0.0446$). (Fig. 3C and D).

3.3.3. *Expression of GSK-3β and CDK5*

Gene expression studies revealed significantly increased expression of GSK-3β (hippocampus: $DF = 3$, $F(3, 8) = 35.92$, $p = 0.0007$) and CDK5 (hippocampus: $DF = 3$, $F(3, 8) = 107.6$, $p < 0.0007$; PFC: $DF = 3$, $F(3, 8) = 85.80$, $p < 0.0001$) in cerebral regions of the AB group compared to the SH group. The EA_{70} and EA_{140} groups showed significant reductions in the GSK-3β expression (hippocampus: $EA_{70:}$ $p = 0.0004$, EA_{140}: $p < 0.0001$ and PFC: $EA_{70:}$ $DF = 3$, $F(3, 8) = 9.456$, $p = 0.0140$, $EA_{140:}$ $p = 0.0064$) and CDK5 expression (hippocampus: $EA_{70:}$ $p < 0.000$, EA_{140}: $p < 0.0001$; PFC: $EA_{70:}$ $p < 0.0001$, $EA_{140:}$ $p < 0.0001$) compared to the AB group (Fig. 3 E).

3.3.4. *Phospho-tau level (p-tau)*

The AB group showed a significant rise in p-Tau levels in the cerebral regions (hippocampus: $DF = 3$, $F(3, 20) = 23.06$, $p < 0.0001$; PFC: $DF = 3$, $F(3, 20) = 96.80$, $p < 0.0001$; AMD: $DF = 3$, $F(3, 20) = 64.48$, $p < 0.0001$) as well as in serum ($DF = 3$, $F(3, 20) = 49.82$, $p < 0.0001$) compared to the SH group. The EA_{70} and EA_{140} groups showed a significant reduction in p-Tau levels in both the cerebral regions (hippocampus: EA_{70}: $p = 0.0012$, EA_{140}: $p < 0.0001$; PFC: EA_{70}: $p < 0.0001$, EA_{140}: $p < 0.0001$; AMD: EA_{70}: $p < 0.0001$, EA_{140}: $p < 0.0001$) and serum (EA_{70}: $p = 0.0048$, EA_{140}: $p < 0.0001$) compared to the AB group (Fig. 3 F).

3.3.5. *Detection of Aβ plaque and tangles*

Silver staining of the rat brain sections revealed the presence of amyloidopathy and NFTs in the cerebral regions. The SH group showed clear and silver stain-negative representations, indicating the absence of amyloidogenic pathology. In contrast, brain sections from the AB group exhibited pathologically abundant senile plaques, including both compact amyloid cores and diffused plaques,

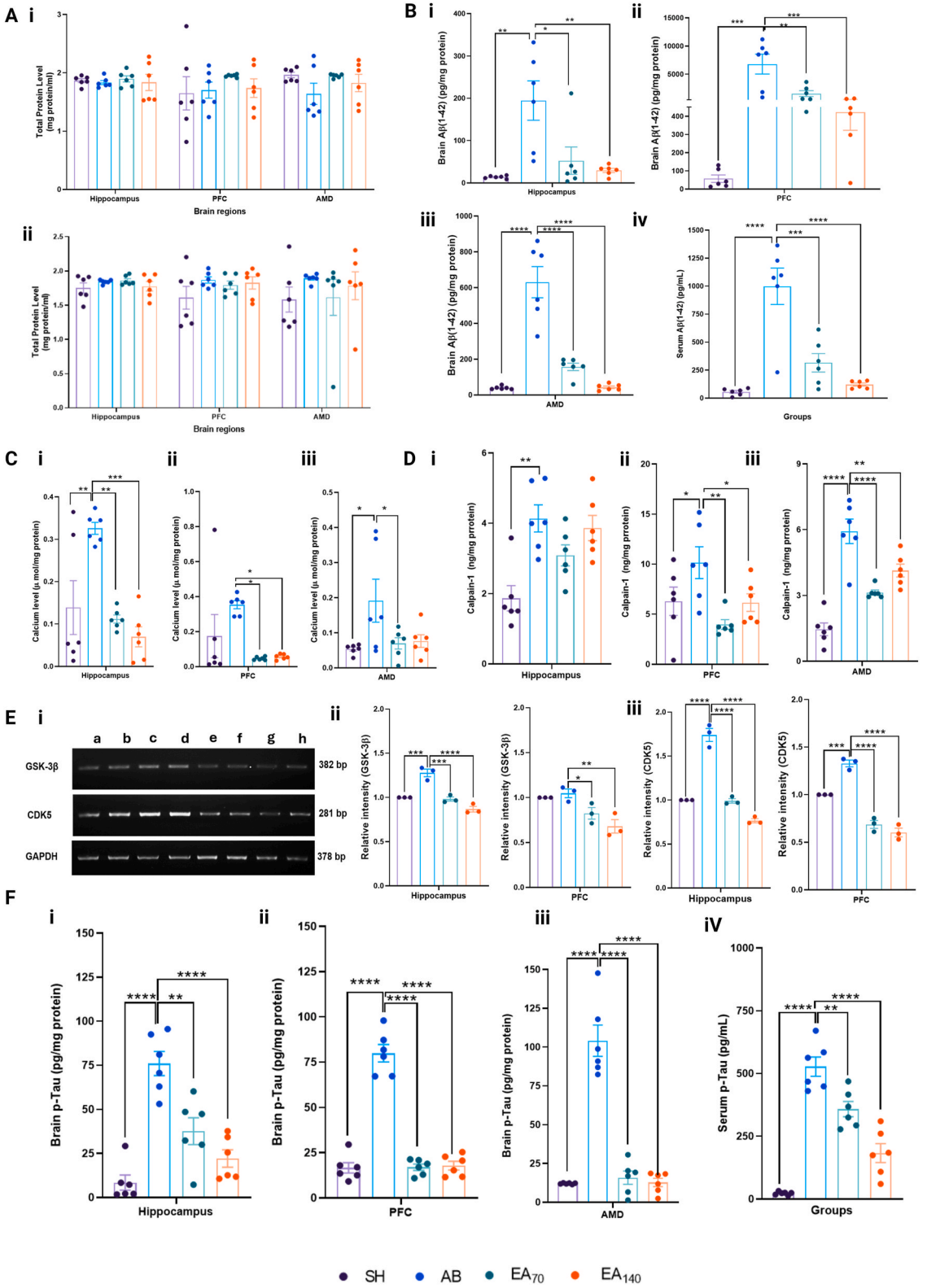

Fig. 3. A) i. Total protein estimation for cerebral peptide levels; ii. Total protein quantification for Ca^{2+} estimation procedure (n = 6). B) Effects of EA treatments on i. hippocampus, ii. PFC, iii. AMD, and iv. serum Aβ levels (n = 6). C) Effects of AB and EA treatments on calcium levels in i. hippocampus, ii. PFC, and iii. AMD (n = 6). D) Effects of AB and EA treatments on brain calpain levels in i. hippocampus, ii. PFC, and iii. AMD (n =

6). E) Effects of AB and EA on the gene expression profile of GSK-3β and CDK5. i) SH: a) Hippocampus, b) PFC; AB: c) Hippocampus, d) PFC; EA70: e) Hippocampus, f) PFC; EA140: g) Hippocampus, h) PFC. mRNA expression of GSK-3β: ii. hippocampus; PFC and CDK5: iii. Hippocampus; PFC, after AB and EA treatments. The relative intensity for each group was calculated relative to the expression profile of the SH group (n = 3). F) Effects of AB and EA treatments on cerebral i. hippocampus, ii. PFC, iii. AMD, and iv. serum p-Tau levels (n = 6). All data are represented as Mean ± SEM. *p < 0.05, **p < 0.01, ***p < 0.001, ****p < 0.0001. Statistical analysis was conducted by one-way ANOVA followed by Dunnett's multiple comparison test.

along with NFTs, and amyloidogenic angiopathy. In the EA_{70}-treated group, brain sections showed an absence of amyloidopathy near the SGZ of the DG. However, amyloidogenic necrosis was observed near the CA1 region. CA2 and CA3 regions displayed NFTs, though their abundance was less than in the AB group. The ERC and PFC regions of EA_{70}-treated brains showed a reduction in diffused plaque and NFTs, whereas AMD showed an absence of such pathology compared to the AB group. Similarly, all brain regions in the EA_{140}-treated group showed a significant reduction in AD pathology compared to the AB group (Fig. 4A–C).

3.4. Effects of EA in AB-induced inflammatory cascade

3.4.1. Astroglial cell activation and GFAP levels

Immunoreactivity with GFAP in rat brain sections indicated the activation of astroglial cells in various cerebral regions. Brain sections from the AB group exhibited a strikingly significant elevation in GFAP-positive cells across all examined areas (DG: DF = 3, F (3, 20) = 106.9, $p < 0.0001$; CA1: DF = 3, F (3, 20) = 20.71, $p < 0.0001$; CA2: DF = 3, F (3, 20) = 69.19, $p < 0.0001$; CA3: DF = 3, F (3, 20) = 218.7, $p < 0.0001$; ERC: DF = 3, F (3, 20) = 250.6, $p < 0.0001$; PFC: DF = 3, F (3, 20) = 319.9, $p < 0.0001$; AMD: DF = 3, F (3, 20) = 68.84, $p < 0.0001$) compared to the SH group. The EA_{70} and EA_{140} groups revealed significantly reduced levels of active astroglial cells in these brain regions (DG: EA_{70}: $p < 0.0001$, EA_{140}: $p < 0.001$; CA1: EA_{70}: $p = 0.0026$, EA_{140}: $p < 0.0001$; CA2: EA_{70}: $p = 0.0012$, EA_{140}: $p < 0.001$; CA3: EA_{70}: $p < 0.0001$, EA_{140}: $p < 0.0001$; ERC: EA_{70}: $p = 0.0002$, EA_{140}: $p < 0.0001$; PFC: EA_{70}: $p < 0.0001$, EA_{140}: $p < 0.0001$; AMD: EA_{70}: $p < 0.0001$, EA_{140}: $p < 0.0001$), as indicated by a reduction in mean GFAP count (Fig. 5C).

3.4.2. TNF-α levels

TNF-α levels were significantly elevated in the cerebral regions (PFC: DF = 3, F (3, 20) = 29.57, $p < 0.0001$; AMD (DF = 3, F (3, 20) = 4.366, $p = 0.0292$) as well as in the serum (DF = 3, F (3, 20) = 26.56, $p < 0.0001$) of the AB group compared to the SH group. A significant reduction in inflammation was indicated by a decrease in TNF-α levels in the cerebral areas (PFC: EA_{70}: $p < 0.0001$, EA_{140}: $p < 0.0001$; AMD: EA_{70}: $p = 0.0239$) and in the serum (EA_{70}: $p < 0.0001$, EA_{140}: $p < 0.0001$) following treatment with EA, compared to the AB group (Fig. 6 A).

3.4.3. Expression of FAIM-L

Gene expression analysis revealed a downregulation of FAIM-L in the hippocampus (DF = 3, F (3, 8) = 0.584, $p = 0.6286$) and prefrontal cortex (PFC) (DF = 3, F (3, 8) = 1.459, $p = 0.3282$) in the AB group compared to the SH group. Although treatment with EA_{70} and EA_{140} resulted in an observed increase in FAIM-L expression, the changes did not reach statistical significance (hippocampus: EA_{70}: $p = 0.9896$, EA_{140}: $p = 0.9954$; PFC: EA_{70}: $p = 0.9998$, EA_{140}: $p = 0.7938$) when compared to the AB group (Fig. 6 B).

3.5. Effects on neuroregulatory markers

3.5.1. CREB levels

The AB group showed a significant reduction in CREB levels in the hippocampus (DF = 3, F (3, 20) = 28.30, $p = 0.0147$) compared to the SH group. Although the visible declination was also seen in PFC (DF = 3, F (3, 20) = 1.395, $p = 0.7827$) and AMD (DF = 3, F (3, 20) = 1.970, $p = 0.5921$), these alterations were statistically insignificant. EA treatment showed an elevation in CREB levels across all three brain regions compared to the AB group. However, a statistically significant elevation was met only in the hippocampus (hippocampus: EA_{70}: $p = 0.4335$, EA_{140}: $p < 0.0001$; PFC: EA_{70}: $p = 0.9906$, EA_{140}: $p = 0.2650$; AMD: EA_{70}: $p = 0.7110$, EA_{140}: $p = 0.9660$) (Fig. 6C).

3.5.2. Dnm-1 expression

The hippocampus (DF = 3, F (3, 8) = 38.46, $p < 0.0001$) and PFC (DF = 3, F (3, 8) = 21.21 $p = 0.0002$) regions of the AB group animals showed a significant downregulation of Dnm-1 levels compared to the SH group. EA treatment significantly upregulated Dnm-1 level in both the hippocampus (EA_{70}: $p = 0.0033$, EA_{140}: $p = 0.0003$) and PFC (EA_{70}: $p = 0.0059$, EA_{140}: $p = 0.0285$) at both dosage levels compared to the AB group (Fig. 6 D).

3.5.3. Synaptophysin levels

Neural synaptic plasticity was markedly reduced in the brains of the AB group, as evidenced by a significant decrease in mean synaptophysin levels across multiple regions (DG: DF = 3, F (3, 20) = 6.613, $p = 0.0204$; CA1: DF = 3, F (3, 20) = 15.87, $p < 0.0001$; CA2: DF = 3, F (3, 20) = 23.09, $p = 0.0091$; CA3: DF = 3, F (3, 20) = 10.16, $p = 0.0167$; ERC: DF = 3, F (3, 20) = 13.18, $p = 0.0380$; PFC: DF = 3, F (3, 20) = 10.63, $p = 0.0032$; AMD: DF = 3, F (3, 20) = 16.89, $p < 0.0001$), indicating Aβ-induced cognitive impairment, reduced learning capacity, and impaired memory retrieval. In the EA_{70}-treated group, a significant increase in mean synaptophysin

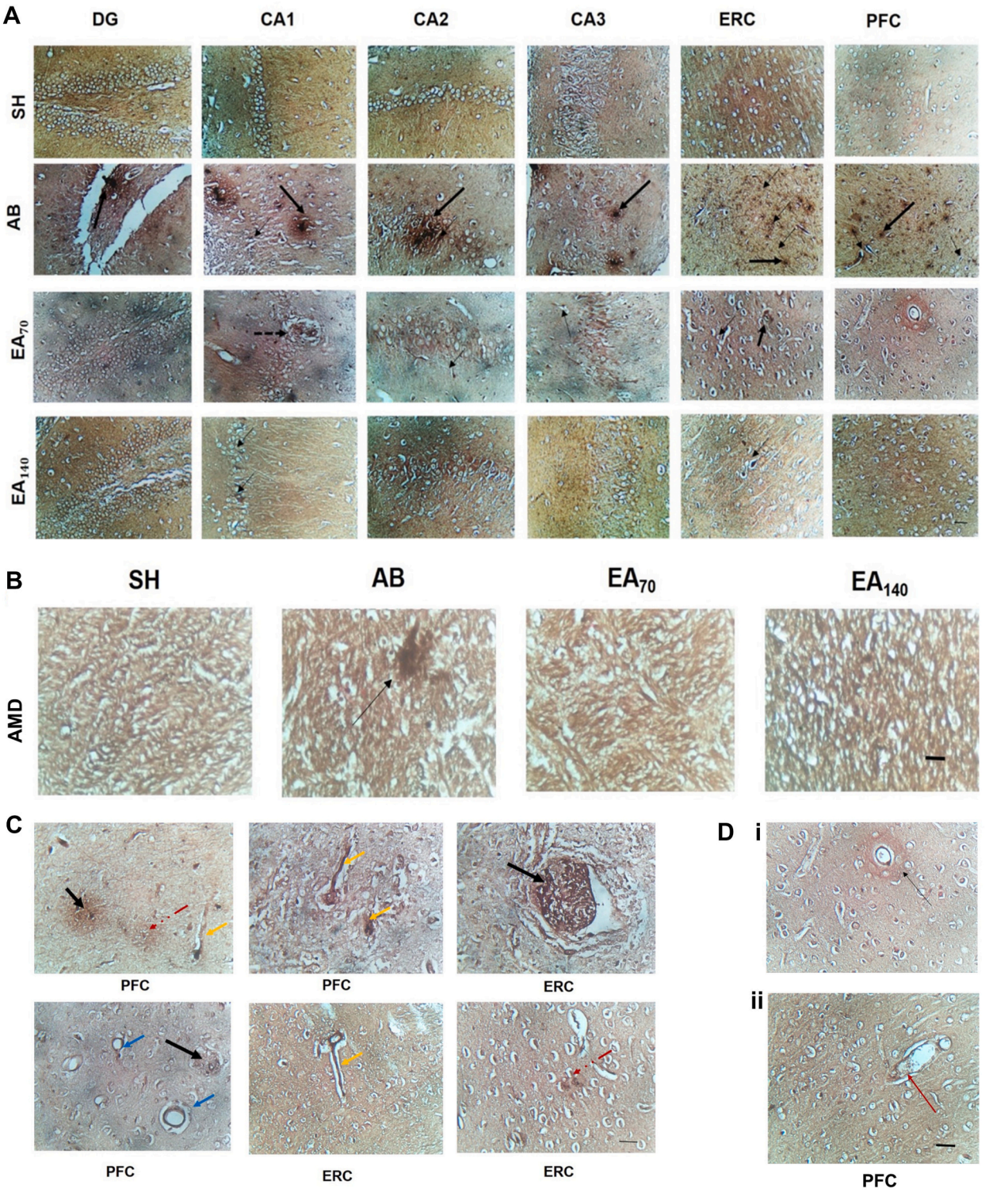

(caption on next page)

Fig. 4. A) Silver staining of rat brain hippocampus proper (DG, CA1, CA2, and CA3), ERC, and PFC. The analysis compares the presence of amyloid plaque (thick black arrow), NFT (thin black arrow), and amyloidogenic necrosis (dotted arrow) in several regions. Magnification: 250×, scale bar: 10 μm. B) Silver staining of rat brain AMD. The analysis compares the presence of amyloid plaque (thin black arrow). Magnification: 400×, scale bar: 10 μm. C) Silver staining of ERC and PFC regions of AD brain. The analysis displays the presence of condensed amyloid plaque (black arrow), diffused plaque (red arrow), NFT (yellow arrow), and amyloidogenic angiopathy (blue arrow). Magnification: 250×, scale bar: 10 μm. D) Silver-stained PFC region of rat brain. i) Black arrow: accumulation of Aβ surrounding the blood vessel; ii) Red arrow: damage of blood vessel and deposition of amyloid plaque within. Magnification: 250×, scale bar: 10 μm.

levels was observed in the ERC ($p = 0.0011$), PFC ($p = 0.0281$), and AMD ($p = 0.0009$). The EA140-treated brains demonstrated a significant elevation in mean synaptophysin levels across all analyzed brain regions (DG: $p = 0.0026$; CA1: $p = 0.0329$; CA2: $p < 0.0001$; CA3: $p = 0.0003$; ERC: $p < 0.0001$; PFC: $p = 0.0001$; AMD: $p = 0.0002$), suggesting a dose-dependent enhancement of synaptic connectivity and neural plasticity with EA treatment (Fig. 7C).

3.6. Effects of EA against Aβ induced cerebral damage and behavioral changes

3.6.1. Protective effects of EA on Aβ induced cerebral damage

Histopathological evaluation revealed a normal cytological profile in the hippocampus, ERC, PFC, and AMD of SH group brains. No signs of pathological deformities, such as cellular atrophy, apoptotic cells with condensed nuclei, or cellular disarrangements, were observed in any of the analyzed regions. The cellular architecture in all the examined areas appeared free from any sign of pathology. In contrast, brain sections from the AB group showed strikingly noteworthy disorganization of GCL in SGZ of DG. The granular cells in DGEC and DGEN were irregularly altered and misaligned compared to the SH group brains. The CA1, CA2, and CA3 regions showed a predominance of apoptotic events and atrophic pyramidal cells. Moreover, The ERC and PFC showed an evident neuronal atrophy and the presence of apoptotic cells with condensed nuclei. Similarly, the AMD in the AB group revealed atypical structural deterioration of intercalated cells. In contrast, brain sections from the EA_{70} and EA_{140} treatment groups revealed strikingly noticeable retardation in pathological changes, including disorganization of cytological architecture, neuronal loss, and apoptosis inside the hippocampus proper, ERC, PFC, and AMD, indicating the neuroprotective virtue of EA (Fig. 8).

3.6.2. Morris Water Maze (MWM)

An RM two-way ANOVA revealed a significant treatment × time interaction effect on escape latency during the acquisition trial phase ($DF = 3$, $F(12, 220) = 1.823$, $p = 0.0459$). Aβ-treated animals demonstrated impaired learning during the acquisition trial, as indicated by an increase in escape latency from day 1 to day 5. On the 4th ($p < 0.0001$) and 5th ($p = 0.0002$) days of the acquisition trial, the AB group showed a significant increase in escape latency, indicating substantial impairment in spatial learning compared to the SH group. In contrast, the EA_{70} (day 4: $p < 0.0001$; day 5: $p < 0.0001$) and EA_{140} (day 4: $p < 0.0001$; day 5: $p < 0.0001$) groups exhibited a significant reduction in escape latency. A significant treatment effect on swimming velocity was also observed between the groups ($DF = 3$, $F(3, 220) = 7.115$, $p = 0.0001$). The AB group did not show any significant changes in swimming velocity at any time point during the acquisition trial phase compared to the SH group. However, animals treated with EA_{70} (day 1: $p = 0.0290$) and EA_{140} (day 5: $p = 0.0262$) displayed significant variations in swimming velocity. Despite these variations, within-group comparisons (day 1 to day 5 of the acquisition trial) revealed no fluctuations in velocity ($F(3.516, 154.7) = 1.462$, $p = 0.2217$), indicating that treatment did not affect motor coordination throughout the study period. The nonsignificant fluctuations in swimming velocity observed in the AB group during inter-day comparisons suggest that no adverse changes in motor coordination occurred during the trial phase. No significant treatment × time interaction effect ($DF = 12$, $F(12, 220) = 1.520$, $p = 0.1181$) was observed on the distance traveled by animals during the acquisition trial phase. However, significant effects of treatment ($DF = 3$, $F(3, 220) = 10.96$, $p < 0.0001$) and day ($DF = 4$, $F(4, 220) = 67.17$, $p < 0.0001$) were observed on the traveled distance. The AB group showed a significant increase in the distance traveled on day 1 ($p = 0.0069$) and day 4 ($p < 0.0001$) compared to the SH group. In contrast, the distance traveled by the EA_{70} (day 4: $p < 0.0001$) and EA_{140} (day 4: $p < 0.0001$) groups was reduced throughout the trial phase, indicating that these animals took less time to reach the platform (Fig. 9A–B).

The locomotion path maps generated during the probe trial provided valuable insights into the animals' spatial memory and retention abilities within the target quadrant. After the 5-day acquisition trial, the AB group demonstrated a significant reduction in time spent in the target quadrant- A ($DF = 3$, $F(3, 44) = 5.597$, $p = 0.0013$), reflecting impaired retrieval of information related to the escape platform. This impairment was further evidenced by a significant increase in escape latency ($DF = 3$, $F(3, 44) = 6.510$, $p = 0.0130$) compared to the SH group. Additionally, the AB group exhibited a marked decrease in the number of crossings over the target quadrant ($DF = 3$, $F(3, 44) = 7.585$, $p = 0.0038$) and a significant decline in memory score ($DF = 3$, $F(3, 44) = 5.289$, $p = 0.0037$). In contrast, animals treated with EA_{70} ($p = 0.0055$) and EA_{140} ($p = 0.0015$) demonstrated a significant reduction in escape latency. EA treatment also led to a significant increase in retention time (EA_{140}: $p = 0.0076$), the number of crossings over the target quadrant (EA_{140}: $p = 0.0005$), and an improvement in memory score (EA_{140}: $p = 0.0146$) compared to the AB group. However, the effects of EA_{70} on retention time ($p = 0.1347$), the number of crossings over the target quadrant ($p = 0.2698$), and memory score ($p = 0.2184$) were not statistically significant. The variations in average swimming velocity ($DF = 3$, $F(3, 44) = 2.059$, $p = 0.1194$) and total distance traveled ($DF = 3$, $F(3, 44) = 2.088$, $p = 0.1155$) were statistically insignificant across all groups (Fig. 9C–D).

3.6.3. Cued/delayed avoidance behavior test for learning and memory

No significant treatment × time interaction effect was observed during the training phase for either cued/delayed conditional

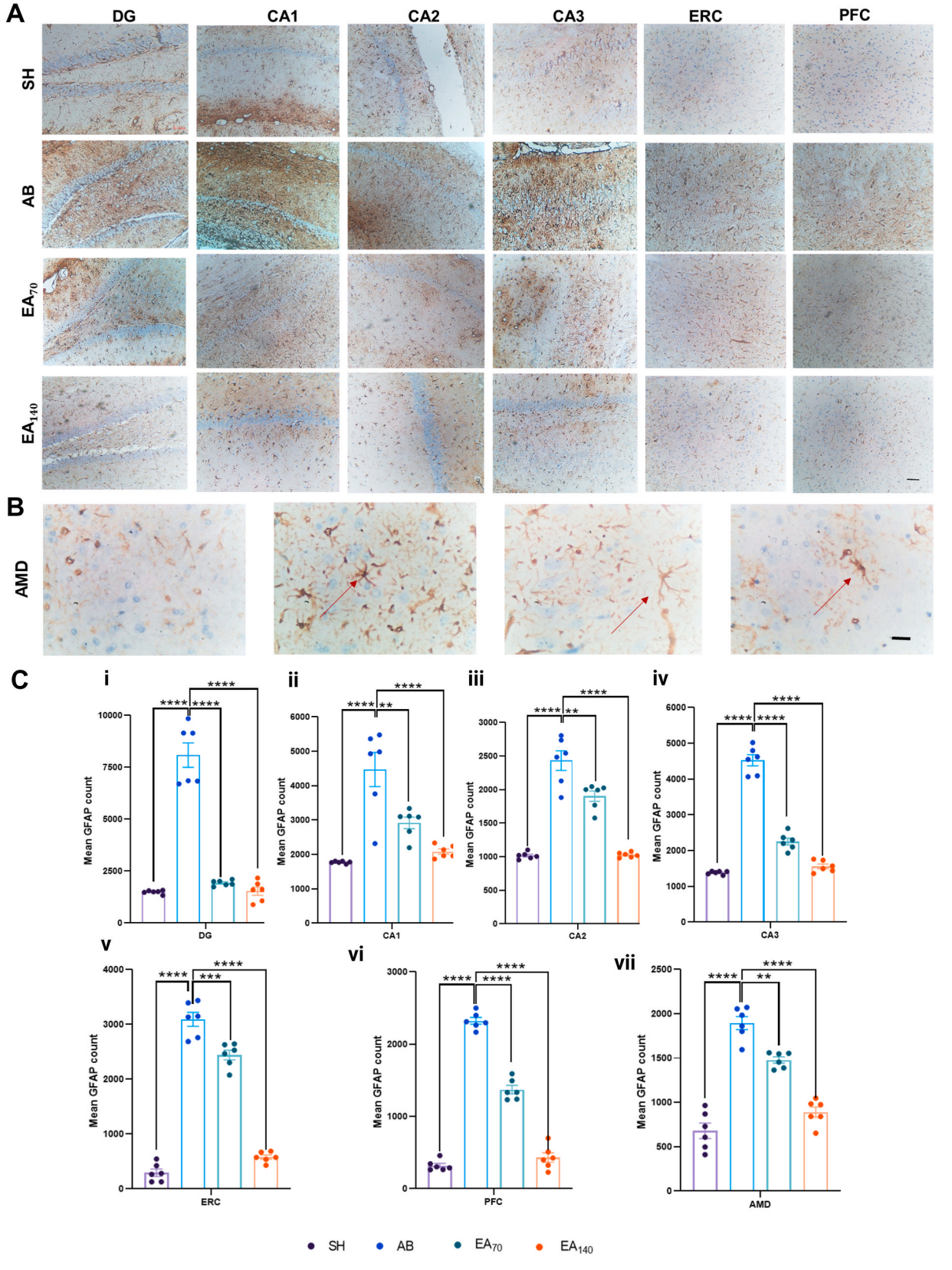

(caption on next page)

Fig. 5. A) GFAP immunolabeling in rat brain hippocampus proper, including DG, CA1, CA2, CA3; ERC, and PFC. Magnification: 100×. B) GFAP immunolabeling in rat brain AMD. Red arrows indicate active astroglial cells. Magnification: 400×, scale bar: 10 μm. C) Mean GFAP count in i) DG, ii) CA1, iii) CA2, iv) CA3, v) ERC, vi) PFC, and vii) AMD regions. All data are represented as Mean ± SEM (n = 6). *p < 0.05, **p < 0.01, ***p < 0.001, ****p < 0.0001. Statistical analysis was conducted using one-way ANOVA followed by Dunnett's multiple comparison test.

avoidance (DF = 12, F (12, 220) = 1.718, p = 0.0644) or latency for pole climbing (DF = 12, F (12, 220) = 0.7196, p = 0.7311). However, a significant effect of time was evident during both tests: cued/delayed conditional avoidance (DF = 4, F (4, 220) = 33.99, p < 0.0001) and latency for pole climbing (DF = 12, F (4, 220) = 61.92, p < 0.0001). These results indicate that animals across all groups successfully learned to avoid the cued/delayed conditioned stimuli and were able to distinguish between conditioned and unconditioned stimuli throughout the training schedule, as reflected by a reduction in latency to climb the pole in response to the sound (conditioned stimulus) (Fig. 10 A).

After induction of AD, in 2 days of retrieval task with the one-day gap, animals from the AB group showed a significant reduction in % cued/delayed conditioned avoidance (day 3: DF = 3, F (3, 44) = 6.259, p = 0.0028), increase in latency to climb pole (day 1: DF = 3, F (3, 44) = 5.125, p = 0.0044; day 3: DF = 3, F (3, 44) = 33.47, p < 0.0001) and increase in the response to unconditional stimuli (day 1: DF = 3, F (3, 44) = 4.535, p = 0.0085; day 3: DF = 3, F (3, 44) = 4.780 p = 0.0048) when compared to the SH group. EA_{70} treatment resulted in a significant increase in the percentage of cued/delayed conditioned avoidance (day 3: p = 0.0026), a decrease in climbing latency (day 3: p < 0.0001), and a marked reduction in responsiveness to the unconditioned stimuli (day 3: p = 0.0198) compared to the AB group. Similarly, EA_{140} treatment significantly enhanced memory retrieval from the training phase, as indicated by an increase in the percentage of cued/delayed conditioned avoidance (day 3: p = 0.0010) and a reduction in the percentage of responses to unconditioned stimuli (day 3: p = 0.0113). Notably, EA_{140} also significantly reduced climbing latency on both day 1 (p < 0.0001) and day 3 (p < 0.0001) compared to the AB group (Fig. 10 B).

4. Discussion

Several studies have reported the lethal effects of i.c.v. administration of Aβ in rats, highlighting oxidative neuronal decay [31], downregulation of cholinergic receptors, elevated astroglial inflammatory signals [32], and the impairment of both short-term and long-term memory [33] through various molecular mechanisms at different dose levels. Despite the availability of FDA-approved drugs for AD, their severe physiological side effects, variability of efficacy across different individuals, high cost, and modest acute benefits have driven the search for safer alternatives to combat such devastating anomaly. In this regard, several phytochemicals/herbal supplements, nutraceuticals, minerals, vitamins, and hormones have been explored for their relative safety and effectiveness [34,35]. Herein, we studied the effect of EA administered i.c.v. at two dose levels - EA_{70} (70 μM) and EA_{140} (140 μM) against Aβ (10 μL, 1 μg/μL, i.c.v.)- induced amyloidogenic neuropathy. We selected brain regions like the hippocampus, ERC, PFC, and AMD due to their critical role in memory formation and their involvement in AD-like pathophysiology. Our research emphasizes four major aspects: a.) Aβ-induced amyloidopathy, subsequent tauopathy, and the involved pathways, b.) neuroinflammatory changes, c.) alteration in neuromodulator pathways, and d.) Histological changes in neural architecture and their impact on the behavioral alterations observed in experimental animals.

The *in-silico* molecular interactions of investigational molecules were compared with the previous findings [29,36–39]. Among all the investigational molecules, EA emerged as the most superior from a polar score perspective, demonstrating the highest polar score and greater affinity at the target site, along with an optimal crash score [40,41]. Although the crash scores of other investigational molecules, such as FA, and cycloartenyl ferulate counterparts of OZ, were closer to zero compared to EA, their lower polar score suggested weaker affinity and interactions with Aβ peptide. Furthermore, EA showed molecular interactions with Lys16, Leu17, and Phe20, which have been reported as the prime cleavage site within the Tyr10-Val24 α-helix of Aβ. These interactions are consistent with previously reported data [37,42], reinforcing the target selectivity of EA against Aβ-induced amyloidopathy. DONO, on the other hand, showed hydrogen bond interaction at His13, a critical residue that, along with Lys16 and other amino acids, forms the Tyr10-Val24 α-helix of Aβ [43]. This interaction is crucial for stabilizing the α-helix and preventing its conversion into the more aggregatory β-sheet form, as previously observed with nicotine [44]. However, DONO's weaker hydrogen-bond interaction renders it less effective as a ligand for Aβ inhibition. The EA showed 507.04, 241.40, and 3.86-fold higher anti-aggregatory effects against Aβ compared to DONO, FA, and OZ respectively, which supports our *in-silico* outcomes. The fundamental mechanism behind the potential of these phenolic moieties to prevent Aβ aggregation lies in their ability to inhibit the latter stages of aggregation, where the oligomeric β sheet (converted from α-helical structure by HFIP treatment) transition into protofibrils and ultimately mature fibrils [29], which is considered as a critical stage in plaque formation in AD. Consequently, the overall evaluation of these investigational therapeutics highlights EA as the most promising molecule of choice for further *in-vivo* studies against Aβ-induced toxicity.

Disturbance in the clearance process of APP-derived Aβ can lead to elevated neuropathological events. In our experiment, biochemical estimation of Aβ in cerebral regions of the SH group unveiled substantial basal levels of Aβ, consistent with the previously published reports [45]. In contrast, the Aβ group exhibited significantly higher deposition of Aβ in both cerebral regions and serum. This cerebral deposition was strongly associated with alterations in the chemical conformation of Aβ by HFIP treatment, transitioning from an α-helical coil to a β-sheet conformation [46], which is more prone to oligomerization, protofibril, and subsequent mature fibril formation [29]. Oligomeric Aβ can either modulate NMDA and VDCC activity, altering the intracellular Ca^{2+} pool or elevate intraneuronal cytoplasmic Ca^{2+} levels by interfering with the ER pool through IP3/RyR signaling [47,48]. In both cases, this leads to elevated glutaminergic drive and subsequent excitotoxicity. Growing evidence suggests that Aβ-mediated rise in calpain-1 levels and

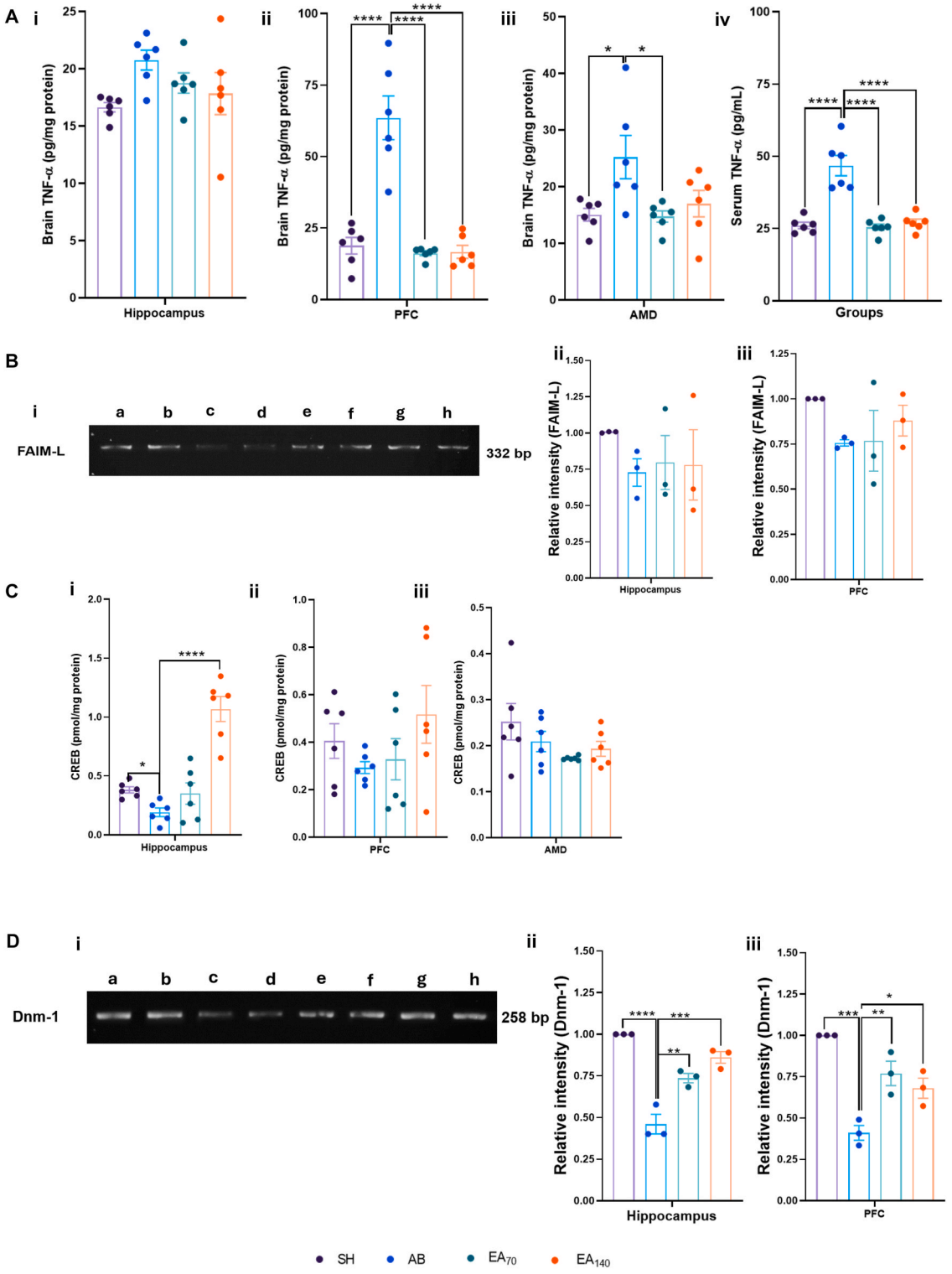

Fig. 6. A) Effects of AB and EA on cerebral i) hippocampus, ii) PFC, iii) AMD, and iv) serum TNF-α levels (n = 6). B) Effects of AB and EA treatments on the i) gene expression profile of FAIM-L. SH: a) Hippocampus, b) PFC; AB: c) Hippocampus, d) PFC; EA70: e) Hippocampus, f) PFC; EA140: g) Hippocampus, h) PFC. mRNA expression of FAIM-L genes in ii) hippocampus and iii) PFC after AB and EA treatments. The relative intensity for each group was calculated relative to the expression profile of the SH group (n = 3). C) Effects of AB and EA treatments on brain CREB levels; i) hippocampus, ii) PFC, and iii) AMD (n = 6). D) Effects of AB and EA on the i) gene expression profile of Dnm-1. SH: a) Hippocampus, b) PFC; AB: c) Hippocampus, d) PFC; EA70: e) Hippocampus, f) PFC; EA140: g) Hippocampus, h) PFC. mRNA expression of Dnm-1 genes in ii) hippocampus and

iii) PFC after AB and EA treatments. The relative intensity for each group was calculated relative to the expression profile of the SH group (n = 3). All data are represented as Mean ± SEM. *p < 0.05, **p < 0.01, ***p < 0.001, ****p < 0.0001. Statistical analysis was conducted using one-way ANOVA followed by Dunnett's multiple comparison test.

activity plays a critical role in AD. There is a bidirectional interplay between Ca^{2+} and calpain-1, as each mutually contributes to altering the other's pool and signaling during neural stress. Aβ-triggered elevation of calpain-1 activity promotes the breakdown of sodium-calcium exchanger-3, augmenting the neurocytoplasmic Ca^{2+} pool, which in turn triggers several cytotoxic events [49,50]. Augmented Ca^{2+} levels also induce conformational changes in calpain-1 proteomics, enhancing its proteolytic activity [51]. Additionally, elevated expression of GSK-3β and activation in the neuronal system is inked with Aβ activity through the downregulation of PI3K signaling [52,53]. Ca^{2+}/calpain-1 activity further truncates GSK-3β at either its C-terminus [54] or N-terminus, removing its inhibitory domain [55] and augmenting its kinase activity. Furthermore, increased CDK5 expression in the AD brain is well-documented [56], with evidence showing its aberrant activation in AD through p25, a truncated product of p35. Calpain-1 promotes the truncation of p35 at its N-terminus and releases p25, which hyperactivates CDK5. Activated GSK-3β has been implicated in the hyperphosphorylation of the microtubule-associated protein tau, elevated Aβ formation, augmented inflammatory events, and memory impairment by disrupting cholinergic signaling [57]. Besides, GSK-3β activity, deregulation of CDK 5 also contributes to hyperphosphorylated tau (p-Tau) formation, with CDK5 phosphorylating tau at multiple Ser/Thr sites [58]. Normally, tau binds to tubulin proteins in microtubules, contributing to neuronal cytoskeleton formation. However, abnormally phosphorylated tau proteins detach from tubulin, misfold, polymerize into paired helical filaments, and ultimately form NFTs [59]. The accumulation of NFTs within neurons potentiates caspase-3-induced apoptosis, leading to neuronal death, a hallmark of AD-associated dementia [60]. Our findings support the cerebral and systemic rise of Aβ and p-Tau levels, followed by vascular trafficking of Aβ in the AB group animals. This may be attributed to reduced concentrations of sLRP1, which sequesters Aβ and alters BBB permeability [61,62]. Accordingly, significantly elevated levels of Ca^{2+}/Calpain-1 and increased expression of GSK-3β and CDK-5 mRNA were observed in the AB group compared to the SH group [63–66]. Silver-stained brain sections provided visual evidence of condensed as well as diffused plaque and the existence of NFTs in the AB group, in contrast to the SH group [67–69].

Astrocytes play a critical role in maintaining cerebral homeostasis by clearing different forms of Aβ through various mechanisms, including transporters like LRP-1, RAGES, and SCARB1, as well as endosomal-lysosomal pathways involving neprilysin, IDE, and MMP9. The clearance pathway selected depends on the phase of transformation in which Aβ exists such as whether monomer, oligomer, or fibril. Aβ plaque deposition makes astroglial cells more reactive, leading to increased inflammation and structural remodeling, characterized by the classic star-shaped morphology of activated astrocytes. These cells begin producing inducible nitric oxide synthase, triggering the formation of nitric oxide and contributing to the synthesis of GFAP [70,71]. Histological analysis of brain sections from Aβ-treated rats revealed a significant number of reactive astroglial cells, evidenced by higher GFAP expression in the hippocampus and AMD compared to SH brain sections. This reflects an inflammatory brain state induced by Aβ-associated amyloidopathy and tauopathy [72]. Upon activation by Aβ-mediated neuropathic biochemical signals, astroglial cells release various inflammatory and pro-inflammatory cytokines into the cerebral environment through activation of astroglial NFκB and FLIP-L dependent ERK/p38MAPK pathways [73,74]. These pathways are associated with increased expression of TNF-α related mRNA and TNF-α production [75–77]. In turn, TNF-α plays a significant role in NFκB and ERK/MAPK-associated survival mechanisms following Aβ overload. While TNF-α has protective roles against Aβ toxicity under homeostatic conditions, in pathological states, its protective effects shift towards degenerative outcomes by promoting apoptotic pathways. The Fas apoptotic inhibitory molecule-L (FAIM-L) is believed to regulate this dual nature by binding to the Fas receptor, antagonizing TNF-α-Fas-driven activation of caspase cascades and preventing apoptotic neuronal death [78]. However, Aβ overload reduces FAIM-L expression, likely due to the formation of Aβ-derived diffusible ligands (ADDLs) during Aβ transformation [79]. Our study aligns with previous findings, showing reduced FAIM-L mRNA expression and increased TNF-α mediated cytotoxicity, alongside elevated numbers of active astroglial cells as evidenced by GFAP immunolabeling in Aβ-treated animals.

LTP and synaptic plasticity depend on the strength and duration of synaptic firing, which are regulated by synaptic vesicle remodeling and replenishment through Dnm-1 mediated GTPase activity. This process promotes the structural and functional retrieval of vesicles through synaptic endocytosis, replenishing the synaptic vesicle pool for subsequent neuronal firing in response to stimuli [80–82]. Previous studies have demonstrated that Dnm-1 depletion occurs following Aβ administration in hippocampal synaptic vesicles [83], and our findings similarly show marked Dnm-1 expression depletion in the hippocampus and PFC compared to the SH group. The role of CREB in LTP, synaptic plasticity, memory consolidation, and neurogenesis is well established [84]. Thus, the reduced CREB expression observed following Aβ exposure likely contributes to compromised neuronal function and is strongly associated with memory dysfunction [85]. Synaptophysin, prevalent in presynaptic nerve endings and incorporated into vesicular membranes, serves as a marker of synaptic plasticity and connectivity [7,86]. In our experiments, cerebral CREB levels were depleted in the AB group compared to the SH group, and this depletion was accompanied by a reduction in synaptophysin count in the hippocampus, ERC, PFC, and AMD, indicating loss of synaptic strength and plasticity essential for memory processes [87]. These findings unequivocally suggest that alterations in synaptic transmission contribute directly to impairments in memory formation [88].

During the 5-day acquisition task in the MWM, the AB group exhibited a significant increase in escape latency and total distance traveled, indicating a failure to learn the navigation path to the target platform [89,90]. This learning impairment was attributed to dysfunction in the ERC [91] and disrupted spatial map development due to a lack of synchronization between the prefrontal cortex PFC and hippocampal functions [92], suggesting a disorganized strategy for finding the escape site. Probe trial evaluations provided additional evidence for the precision and strength of long-term memory formation during the 5-days of acquisition trial phase [93].

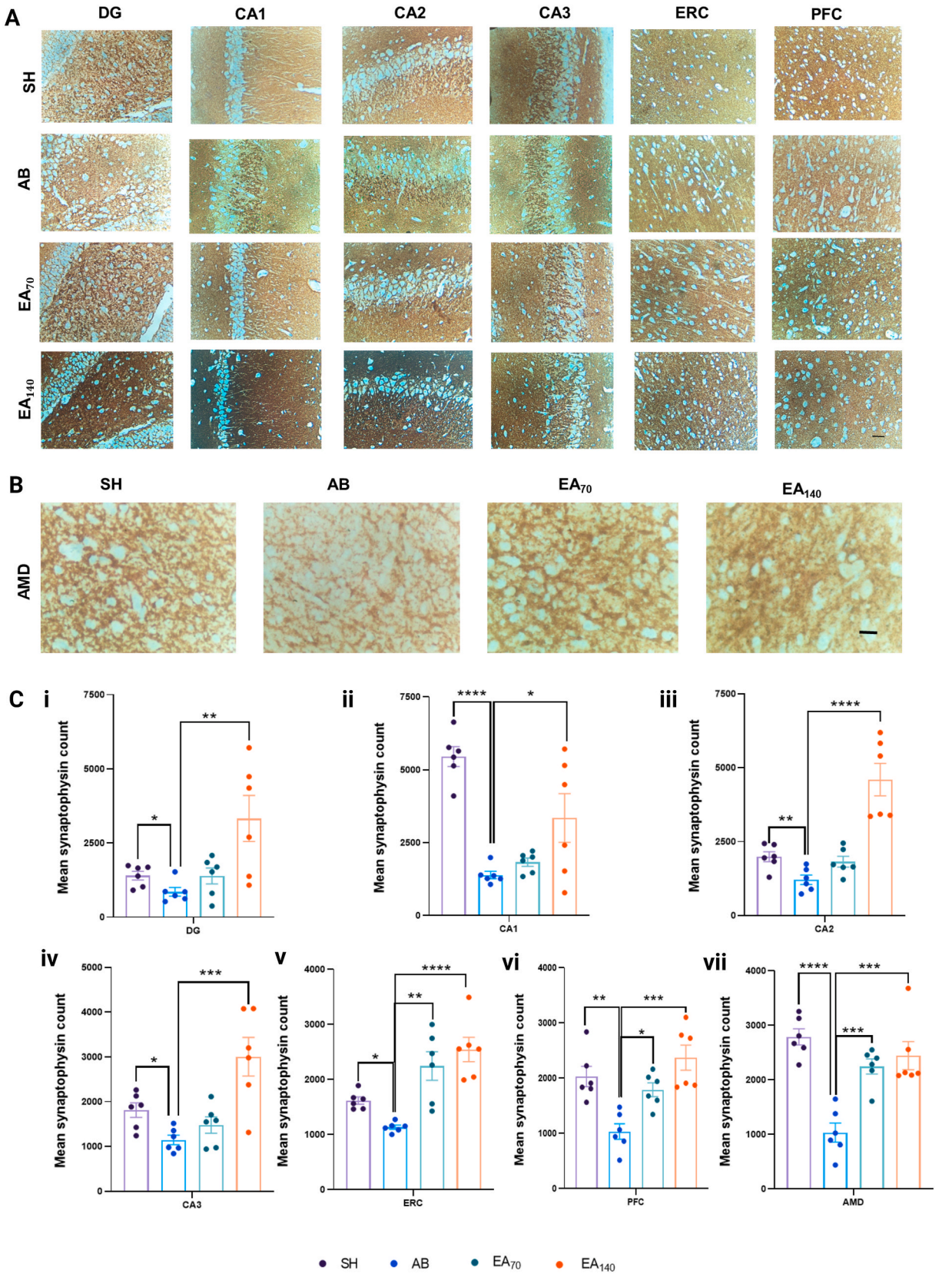

(caption on next page)

Fig. 7. A) Synaptophysin immunolabeling in rat brain hippocampus proper, including DG, CA1, CA2, CA3, ERC, and PFC regions. Magnification: 250×. B) Synaptophysin immunolabeling in the rat brain AMD region. Magnification: 400×, scale bar: 10 μm. C) Mean synaptophysin count in i) DG, ii) CA1, iii) CA2, iv) CA3, v) ERC, vi) PFC, and vii) AMD regions. All data are represented as Mean ± SEM (n = 6). *p < 0.05, **p < 0.01, ***p < 0.001, ****p < 0.0001. Statistical analysis was conducted using one-way ANOVA followed by Dunnett's multiple comparison test.

Neuronal decay in the PFC was associated with a loss of retrieval ability for learned spatial memory during both the acquisition and probe trials, as evidenced by swim path observations [92,94]. These anomalies manifested as increased latency to reach the target quadrant, reduced time spent, and fewer crossings in the target quadrant during the probe trial. The swimming velocity and distance traveled by AB animals did not significantly alter, suggesting that cognitive impairments were independent of changes in swimming ability and reflected a loss of spatial-cognitive memory rather than functional memory [95]. The associative learning task helped to ascertain the mechanisms involved in discrete learning processes, particularly the roles of the hippocampus, PFC, and AMD. Associative learning, an adaptive behavior that enables the subject to anticipate and respond to expected upcoming events [96], was impaired in Aβ-treated animals, as they failed to retrieve conditional cue-linked memories during the 1st and 3rd day retrieval tasks. This failure suggests an inability to recognize CS and associate them with aversive UCS such as shocks. Beyond hippocampal [97] and PFC [98] damage, histopathological disorganization in intercalated cells, amyloid plaque formation, and positive alterations in biochemical, genetic, and immunohistochemical parameters were observed in the AMD [99,100], likely contributing to impaired associative learning-dependent plasticity.

The effects of EA in reducing Aβ-associated pathology are well-documented [101], but its role in preventing tau hyperphosphorylation, which follows amyloidopathy and leads to neuronal death, remains unclear. Previous studies have shown that EA has a Ca^{2+}-chelating effect [102], which may influence the intracellular Ca^{2+}- gradient and modulate interactions between Ca^{2+} and related proteins by inducing conformational changes. EA can also affect receptor and ion channel conformation, regulating Ca^{2+} entry

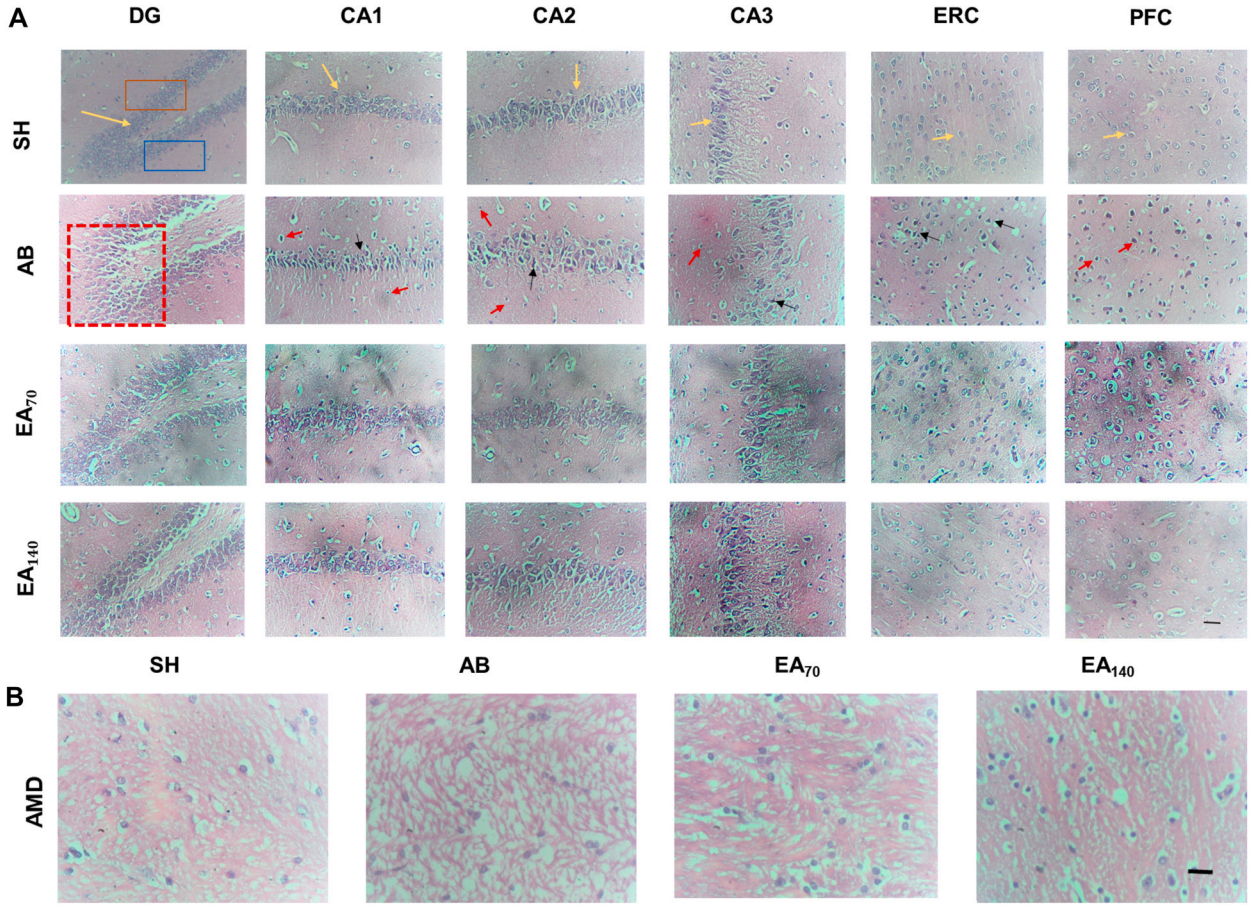

Fig. 8. A) H&E staining of hippocampus proper, including DG, CA1, CA2, CA3, ERC, and PFC regions. Histopathological analysis reveals live cells (yellow arrow), significant alterations in the thickness of the pyramidal cell layer and neuronal loss/dead cells (black arrows) in CA regions, altered granular cell arrangement in the DG area of the hippocampus (red dotted box), and apoptotic cells (red arrow). The orange rectangle highlights comparisons between DGEC, and the blue rectangle highlights comparisons between DGEN of the DG arm, magnification 250×. B) H&E staining of the rat amygdala, magnification 400×, scale bar: 10 μm.

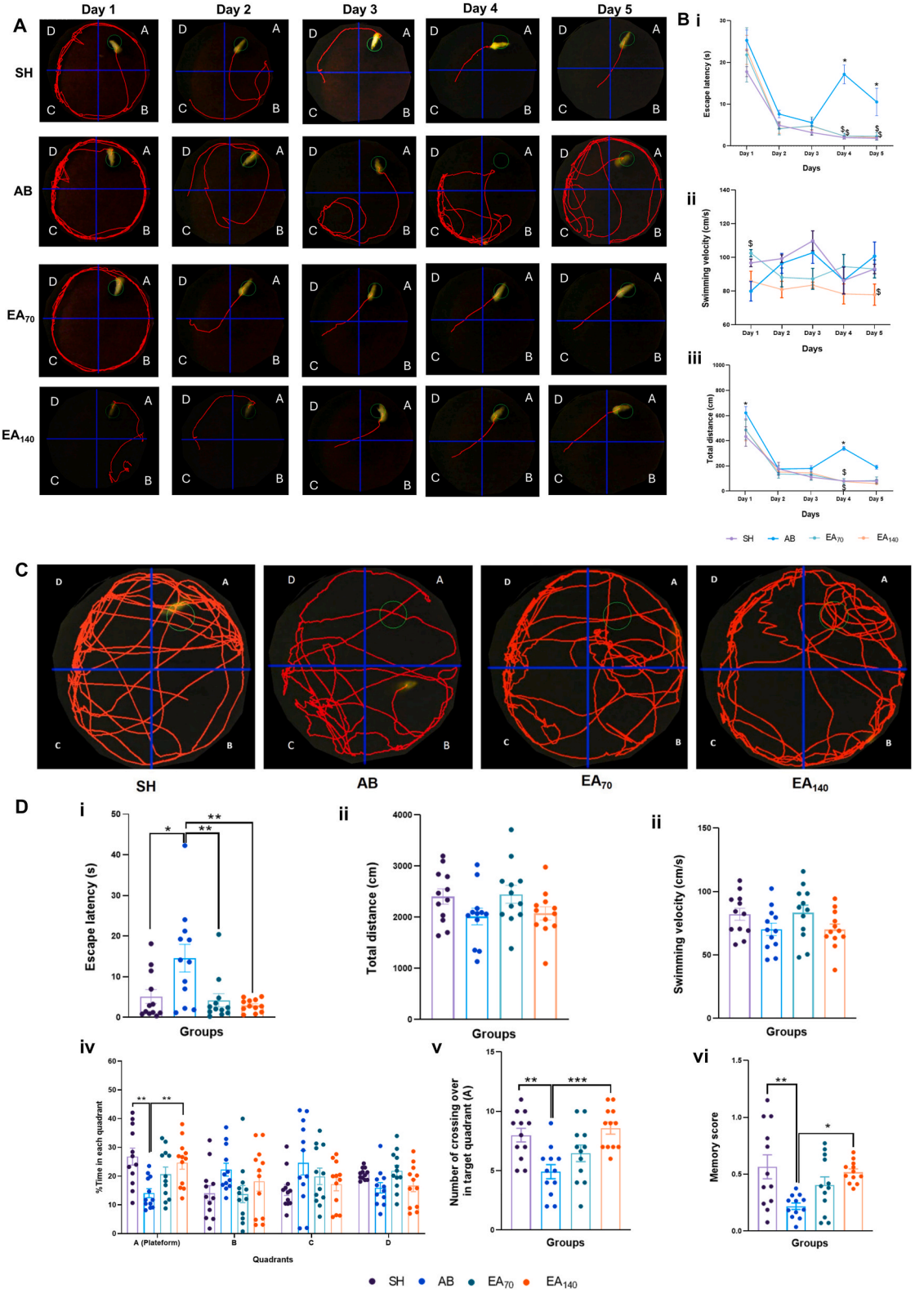

Fig. 9. A) Navigation path during the acquisition trial after treatment with AB, EA70, and EA140 from day 1 to day 5. B) i. Escape latency (s); ii. Swimming velocity (cm/s); and iii. Total distance traveled during the acquisition trial phase. All data are presented as Mean ± SEM (n = 12). Statistical differences between groups were evaluated using one-way ANOVA followed by Dunnett's multiple comparison test for each day. *p <

0.05 vs SH and $p < 0.05 vs AB. C) Navigation path during the probe trial after treatment with AB, EA70, and EA140. D) Effects of EA treatment on spatial reference memory and motor functionality in AB-induced AD. i. Escape latency; ii. Total distance; iii. Swimming velocity; iv. % time in each quadrant; v. Number of crossings over in the target quadrant (A); and vi. Memory score during the probe trial. All data are presented as Mean ± SEM (n = 12). *p < 0.05, **p < 0.01, ***p < 0.001, ****p < 0.0001. Statistical analysis was conducted using one-way ANOVA followed by Dunnett's multiple comparison test.

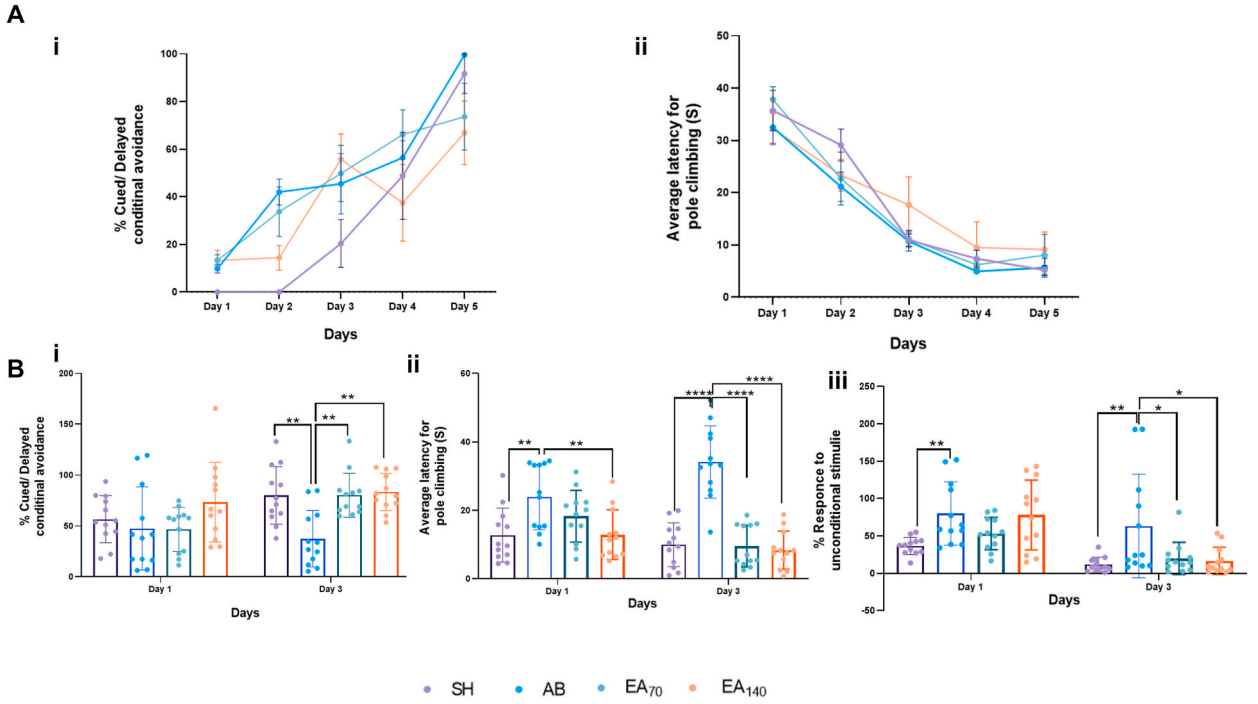

Fig. 10. A.) Conditional Avoidance Behavior of Animals During Training Period. i.) % Cued/Delayed Conditional Avoidance and ii.) Average Latency for Pole Climbing. Statistical differences between groups were evaluated using one-way ANOVA followed by Dunnett's multiple comparison test for each day. *p < 0.05 vs SH and $p < 0.05 vs AB. B.) Effects of AB and EA Treatments on Conditioned Avoidance Behavior of AD Rats During Retrieval Task. i.) % Cued/Delayed Conditional Avoidance; ii.) Average Latency for Pole Climbing; and iii.) % Response to Unconditional Stimuli. All data are represented as Mean ± SEM (n = 12). *p < 0.05, **p < 0.01, ***p < 0.001, ****p < 0.0001. Statistical analysis was conducted using one-way ANOVA followed by Dunnett's multiple comparison test for each day.

into cells and subsequent signaling cascades [103]. Additionally, EA has been documented to retard intracellular Ca^{2+} levels in rat peritoneal mast cells [104] and selenite-induced cataract lenses [105] by inhibiting Ca^{2+} release from endoplasmic/sarcoplasmic reticulum stores and attenuating voltage-gated Ca^{2+} influx [104]. Our study supports these findings, demonstrating that EA_{70} and EA_{140} treatments retard cerebral Ca^{2+} levels in rats compared to the AB group. Furthermore, calpain-1 levels were reduced in the analyzed cerebral regions at both doses, and decreased GSK-3β and CDK-5 expression were observed, leading to reduced p-tau levels in both cerebral regions and serum. This reduction in NFTs across explored brain regions supports EA-mediated neuroprotection against neuronal death following tauopathy, likely due to initial inhibition of Aβ and Ca^{2+}-derived signaling cascades. The anti-inflammatory effects of EA, which are known to protect against neurodegenerative events by downregulating NFκB/MAPK/TNF-α signaling, are well established [106–109]. Treatment with EA_{70} and EA_{140} significantly reduced cerebral and serum TNF-α levels and elevated FAIM-L mRNA expression in the hippocampus and PFC. Additionally, the reduction in active astroglial cells, evidenced by decreased GFAP count in the hippocampus, PFC, ERC, and AMD, confirmed EA-mediated protection against inflammatory signals and subsequent prevention of neurodegeneration in response to Aβ. This was achieved through the reduction of TNF-α levels, correction of irregular astrocyte signaling, elevation of FAIM-L mRNA expression, and retardation of apoptotic signaling.

The protective role of EA in LTP, synaptic plasticity, and cognitive function restoration has become increasingly evident, particularly following its evaluation in experimental traumatic brain injury models [110]. Treatment with EA, at both dose levels, resulted in a marked elevation in CREB levels, an increased mean synaptophysin count, and upregulation of Dnm-1 gene expression. These findings strongly support the hypothesis that EA mitigates neuronal dysfunction following Aβ exposure. Treatment with EA_{70} and EA_{140} significantly reduced structural disorientation and cellular decay within the hippocampal formation. This preservation of hippocampal integrity suggests that memory acquisition, LTP, memory retention, synaptic plasticity, and relearning abilities were maintained, as evidenced by the animals' behavioral performance during assessment [111]. Moreover, enhanced navigational performance mediated by the ERC and improved memory recall mediated by the PFC were observed. These improvements were

demonstrated by a reduction in path length and latency to reach the target during the acquisition task, as well as increased time spent and entries into the target quadrant during the probe trial. These outcomes suggest the utilization of a more effective spatial orientation strategy to locate the target platform, aligning with findings from previous studies [112–115]. Additionally, the EA_{70} and EA_{140} groups exhibited a significantly shorter latency to climb the pole and a higher percentage of avoidance responses following conditioned stimuli, indicating an enhanced ability to recall the association between the CS and UCS compared to the AB group. These effects are likely due to the enhancement of LTP and synaptic connectivity, achieved through the preservation of both structural and functional aspects of the hippocampus, PFC, and AMD. Previous studies have also supported the neuroprotective effects of EA [116].

5. Research limitations

While this study provides valuable insights into the effect of EA on the symptoms of early-onset Alzheimer's disease through behavioral and physiological correlation, several limitations must be acknowledged. These include limited no of sample size, experimental conditions, or methodological constraints. These factors may influence the generalizability of the results, and further research can be conducted to address these limitations and build upon the findings presented here.

6. Conclusion

Administration of EA at two dose levels demonstrated significant positive effects on cytoprotection, biochemical alterations, gene expression, and behavioral outcomes. These effects were linked to the inhibition of Aβ (1-42) aggregation, Ca^{2+} scavenging, reduction of calpain-1 activity, and regulation of GSK-3β and CDK5 gene expression, which collectively contributed to anti-tauopathy effects. Additionally, EA modulated inflammatory pathways by inhibiting astroglial activation, regulating FAIM-L gene expression, and reducing TNF-α levels. Moreover, EA influenced neuroregulatory pathways, particularly through the Dnm-1/CREB signaling axis, leading to improved synaptic connectivity and enhanced LTP. These neuroprotective effects were evident in the animals' performance during memory acquisition and retrieval tasks in the MWM and in cued/delayed conditioned fear avoidance tasks.

Data availability statement

No data was used for the research described in the article.

CRediT authorship contribution statement

Abhishek B. Jha: Writing – review & editing, Writing – original draft, Visualization, Validation, Software, Resources, Project administration, Methodology, Investigation, Formal analysis, Data curation, Conceptualization. **Udit J. Chaube:** Writing – review & editing, Validation, Software, Formal analysis. **Ashish B. Jha:** Formal analysis.

Declaration of competing interest

The authors declare that they have no known competing financial interests or personal relationships that could have appeared to influence the work reported in this paper.

Acknowledgements

The current research is part of the doctoral studies of Mr. Abhishek B. Jha. The authors would like to acknowledge the Institute of Pharmacy, Nirma University, Ahmedabad, and the Indian Institute of Technology, Gandhinagar, for providing the facilities to conduct this research. Special thanks go to Dr. Hardik Bhatt for his assistance in interpreting the *in-silico* docking results.

References

[1] M.P. Murphy, H. LeVine, Alzheimer's disease and the β-amyloid peptide, J Alzheimers Dis 19 (2010) 311, https://doi.org/10.3233/JAD-2010-1221.
[2] S.M. de la Monte, Brain insulin resistance and deficiency as therapeutic targets in Alzheimer's disease, Curr. Alzheimer Res. 9 (2012) 35–66, https://doi.org/10.2174/156720512799015037.
[3] J.K. Chambers, K. Uchida, T. Harada, M. Tsuboi, M. Sato, M. Kubo, H. Kawaguchi, N. Miyoshi, H. Tsujimoto, H. Nakayama, Neurofibrillary tangles and the deposition of a beta amyloid peptide with a novel N-terminal epitope in the brains of wild Tsushima leopard cats, PLoS One 7 (2012) 2–11, https://doi.org/10.1371/journal.pone.0046452.
[4] J. Dorszewska, M. Prendecki, A. Oczkowska, M. Dezor, W. Kozubski, Molecular basis of familial and sporadic Alzheimer's disease, Curr. Alzheimer Res. 13 (2016) 952–963, https://doi.org/10.2174/1567205013666160314150501.
[5] S.B. Ghatak, S.S. Panchal, Renoprotective effects of oryzanol in an animal model of experimentally induced diabetic nephropathy, Oriental Pharmacy and Experimental Medicine 14 (2013) 55–67, https://doi.org/10.1007/s13596-013-0119-1.
[6] M. Sohail, A. Rakha, M.S. Butt, M.J. Iqbal, S. Rashid, Rice bran nutraceutics: a comprehensive review, Crit. Rev. Food Sci. Nutr. 8398 (2016), https://doi.org/10.1080/10408398.2016.1164120, 00–00.
[7] A.B. Jha, S.S. Panchal, Neuroprotection and cognitive enhancement by treatment with γ-oryzanol in sporadic Alzheimer's disease, J. Appl. Biomed. 15 (2017) 265–281, https://doi.org/10.1016/j.jab.2017.05.001.
[8] Y.P.C. Rao, D. Sugasini, B.R. Lokesh, Dietary gamma oryzanol plays a significant role in the anti-inflammatory activity of rice bran oil by decreasing pro-inflammatory mediators secreted by peritoneal macrophages of rats, Biochem. Biophys. Res. Commun. 479 (2016) 747–752.

[9] S.B. Ghatak, S.J. Panchal, Investigation of the immunomodulatory potential of oryzanol isolated from crude rice bran oil in experimental animal models, Phytother Res. 26 (2012) 1701–1708.

[10] J. Teixeira, A. Gaspar, E.M. Garrido, J. Garrido, F. Borges, Hydroxycinnamic acid antioxidants: an electrochemical overview, BioMed Res. Int. (2013) 1–11, https://doi.org/10.1155/2013/251754, 2013.

[11] Y. Pan, L. Cai, S. He, Z. Zhang, Pharmacokinetics study of ferulic acid in rats after oral administration of γ-oryzanol under combined use of Tween 80 by LC/MS/MS, Eur. Rev. Med. Pharmacol. Sci. 18 (2014) 143–150.

[12] F. Tsai, L. Wu, S. Yang, H. Cheng, Ferulic acid reverses the cognitive dysfunction caused by amyloid β peptide 1-40 through anti-oxidant activity and cholinergic activation in rats, Am. J. Chin. Med. 43 (2015) 1–17, https://doi.org/10.1142/S0192415X15500214.

[13] S. Sarkar, A.A. Siddiqui, S. Mazumder, R. De, S.J. Saha, C. Banerjee, M.S. Iqbal, S. Adhikari, A. Alam, S. Roy, U. Bandyopadhyay, Ellagic acid, a dietary polyphenol, inhibits tautomerase activity of human macrophage migration inhibitory factor and its pro-inflammatory responses in human peripheral blood mononuclear cells, J. Agric. Food Chem. 63 (2015) 4988–4998, https://doi.org/10.1021/acs.jafc.5b00921.

[14] T. Ahmed, W.N. Setzer, S.F. Nabavi, I.E. Orhan, N. Braidy, E. Sobarzo-Sanchez, S.M. Nabavi, Insights into effects of ellagic acid on the nervous system: a mini review, Curr. Pharmaceut. Des. 22 (2016) 1350–1360, https://doi.org/10.2174/1381612822666160125114503.

[15] R. Spitzer, A.E. Cleves, R. Varela, A.N. Jain, Protein function annotation by local binding site surface similarity, Proteins: structure, Function and Bioinformatics 82 (2014) 679–694, https://doi.org/10.1002/prot.24450.

[16] K. Stierand, P.C. Maaß, M. Rarey, Molecular complexes at a glance: automated generation of two-dimensional complex diagrams, Bioinformatics 22 (2006) 1710–1716.

[17] K. Ono, M. Hirohata, M. Yamada, Ferulic acid destabilizes preformed beta-amyloid fibrils *in vitro*, Biochem. Biophys. Res. Commun. 336 (2005) 444–449, https://doi.org/10.1016/j.bbrc.2005.08.148.

[18] S. Mehan, R. Kaur, S. Parveen, D. Khanna, S. Kalra, Polyphenol ellagic acid-targeting to brain: a hidden treasure, International Journal of Neurology Research 1 (2015) 141–152, https://doi.org/10.17554/j.issn.2313-5611.2015.01.20.

[19] D. Yanagisawa, H. Taguchi, S. Morikawa, T. Kato, K. Hirao, N. Shirai, I. Tooyama, Novel curcumin derivatives as potent inhibitors of amyloid β aggregation, Biochem Biophys Rep 4 (2015) 357–368, https://doi.org/10.1016/j.bbrep.2015.10.009.

[20] A. Castro, A. Martinez, Targeting beta-amyloid pathogenesis through acetylcholinesterase inhibitors, Curr. Pharmaceut. Des. 12 (2006) 4377–4387, https://doi.org/10.2174/138161206778792985.

[21] M. Pourmir, P. Babaei, B.S. Tehrani, Kisspeptin - 13 ameliorates memory impairment induced by streptozotocin in male rats via cholinergic system, Physiology and Pharmacology 20 (2016) 38–47.

[22] R.S. Wong, D.F. Cechetto, S.N. Whitehead, Assessing the effects of acute amyloid β oligomer exposure in the rat, Int. J. Mol. Sci. 17 (2016) 1–13, https://doi.org/10.3390/ijms17091390.

[23] C. V Vorhees, M.T. Williams, Morris water maze: procedures for assessing spatial and related forms of learning and memory, Nat. Protoc. 1 (2006) 848–858, https://doi.org/10.1038/nprot.2006.116.

[24] T.G. Heffner, J.A. Hartman, L.S. Seiden, A rapid method for the regional dissection of the rat brain, Pharmacol. Biochem. Behav. 13 (1980) 453–456.

[25] G.J. Gage, D.R. Kipke, W. Shain, Whole animal perfusion fixation for rodents, J. Vis. Exp. (2012) e3564, https://doi.org/10.3791/3564.

[26] A.B. Jha, S.S. Panchal, Neuroprotection and cognitive enhancement by treatment with γ-oryzanol in sporadic Alzheimer's disease, J. Appl. Biomed. (2017) 1–17, https://doi.org/10.1016/j.jab.2017.05.001.

[27] C. Karthick, S. Periyasamy, K.S. Jayachandran, M. Anusuyadevi, Intrahippocampal administration of ibotenic acid induced cholinergic dysfunction via NR2A/NR2B expression: implications of resveratrol against Alzheimer disease pathophysiology, Front. Mol. Neurosci. 9 (2016) 1–16, https://doi.org/10.3389/fnmol.2016.00028.

[28] L.G. Luna, Manual of Histologic Staining Methods of the Armed Forces Institute of Pathology, Blakiston Division, McGraw-Hill, 1968.

[29] K. Ono, L. Li, Y. Takamura, Y. Yoshiike, L. Zhu, F. Han, X. Mao, T. Ikeda, J.I. Takasaki, H. Nishijo, A. Takashima, D.B. Teplow, M.G. Zagorski, M. Yamada, Phenolic compounds prevent amyloid β-protein oligomerization and synaptic dysfunction by site-specific binding, J. Biol. Chem. 287 (2012) 14631–14643, https://doi.org/10.1074/jbc.M111.325456.

[30] G.R. Frost, Y. Li, G.R. Frost, The role of astrocytes in amyloid production and Alzheimer ' s disease, Open Biol 7 (2017) 1–14, https://doi.org/10.1098/rsob.170228.

[31] J.G. McLarnon, J.K. Ryu, Relevance of Aβ 1-42 intrahippocampal injection as an animal model of inflamed Alzheimer's disease brain, Curr. Alzheimer Res. 5 (2008) 475–480.

[32] R.Y. Liu, R. Gu, X.L. Qi, T. Zhang, Y. Zhao, Y. He, J.J. Pei, Z.Z. Guan, Decreased nicotinic receptors and cognitive deficit in rats intracerebroventricularly injected with beta-amyloid peptide(1-42) and fed a high-cholesterol diet, J. Neurosci. Res. 86 (2008) 183–193, https://doi.org/10.1002/jnr.21463.

[33] K. Yamada, T. Tanaka, D. Han, K. Senzaki, T. Kameyama, T. Nabeshima, Protective effects of idebenone and α-tocopherol on β-amyloid-(1–42)-induced learning and memory deficits in rats: implication of oxidative stress in β-amyloid-induced neurotoxicity *in vivo*, Eur. J. Neurosci. 11 (1999) 83–90.

[34] K.A. Wollen, Alzheimer's disease: the pros and cons of pharmaceutical, nutritional, botanical, and stimulatory therapies, with a discussion of treatment strategies from the perspective of patients and practitioners, Alternative Med. Rev. 15 (2010) 223–244.

[35] J. Kim, H.J. Lee, K.W. Lee, Naturally occurring phytochemicals for the prevention of Alzheimer's disease, J. Neurochem. 112 (2010) 1415–1430, https://doi.org/10.1111/j.1471-4159.2009.06562.x.

[36] E. Gowing, A.E. Roher, A.S. Woods, R.J. Cotter, M. Chaney, S.P. Little, M.J. Ball, Chemical characterization of Aβ 17-42 peptide, a component of diffuse amyloid deposits of Alzheimer disease, J. Biol. Chem. 269 (1994) 10987–10990.

[37] H.Y. Shao, S.C. Jao, K. Ma, M.G. Zagorski, Solution structures of micelle-bound amyloid b-(1-40) and b-(1-42) peptides of Alzheimer's disease, J. Mol. Biol. 285 (1999) 755–773.

[38] C.C. Curtain, F. Ali, I. Volitakis, R.A. Cherny, R.S. Norton, K. Beyreuther, C.J. Barrow, C.L. Masters, A.I. Bush, K.J. Barnham, Alzheimer's disease amyloid-β binds copper and Zinc to generate an allosterically ordered membrane-penetrating structure containing superoxide dismutase-like subunits, J. Biol. Chem. 276 (2001) 20466–20473, https://doi.org/10.1074/jbc.M100175200.

[39] D. Giulian, L.J. Haverkamp, J.H. Yu, M. Karshin, D. Tom, J. Li, A. Kazanskaia, J. Kirkpatrick, A.E. Roher, The hhqk domain of beta-amyloid provides a structural basis for the immunopathology of alzheimers-disease, J. Biol. Chem. 273 (1998) 29719–29726, https://doi.org/10.1074/jbc.273.45.29719.

[40] D. Chen, N. Oezguen, P. Urvil, C. Ferguson, S.M. Dann, T.C. Savidge, Regulation of protein-ligand binding affinity by hydrogen bond pairing, Sci. Adv. 2 (2016) 1–16, https://doi.org/10.1126/sciadv.1501240.

[41] Surflex Platform Manual, A Biopharmics Llc Publication, 2018, p. 31.

[42] M. Rogeberg, C.B. Furlund, M.K. Moe, T. Fladby, Identification of peptide products from enzymatic degradation of amyloid beta, Biochimie 105 (2014) 206–220, https://doi.org/10.1016/j.biochi.2014.06.023.

[43] D.A. Butterfield, R. Sultana, Methionine-35 of A β (1–42): importance for oxidative stress in Alzheimer disease, J. Amino Acids 2011 (2011) 1–10, https://doi.org/10.4061/2011/198430.

[44] A.R. Salomon, K.J. Marcinowski, R.P. Friedland, M.G. Zagorski, Nicotine inhibits amyloid formation by the β-peptide, Biochemistry 35 (1996) 13568–13578, https://doi.org/10.1021/bi9617264.

[45] L.A. Pattanashetti, A.D. Taranalli, V. Parvatrao, R.H. Malabade, D. Kumar, Evaluation of neuroprotective effect of quercetin with donepezil in scopolamine-induced amnesia in rats, Indian J. Pharmacol. 49 (2018) 60–64, https://doi.org/10.4103/0253-7613.201016.

[46] S.K. Pachahara, N. Chaudhary, C. Subbalakshmi, R. Nagaraj, Hexafluoroisopropanol induces self-assembly of β-amyloid peptides into highly ordered nanostructures, J. Pept. Sci. 18 (2012) 233–241, https://doi.org/10.1002/psc.2391.

[47] E. Ferreiro, C.R. Oliveira, C.M.F. Pereira, The release of calcium from the endoplasmic reticulum induced by amyloid-beta and prion peptides activates the mitochondrial apoptotic pathway, Neurobiol. Dis. 30 (2008) 331–342, https://doi.org/10.1016/j.nbd.2008.02.003.

[48] C. Supnet, I. Bezprozvanny, The dysregulation of intracellular calcium in Alzheimer disease, Cell Calcium 47 (2010) 183–189, https://doi.org/10.1016/j.ceca.2009.12.014.

[49] J. Atherton, K. Kurbatskaya, M. Bondulich, C.L. Croft, C.J. Garwood, R. Chhabra, S. Wray, A. Jeromin, D.P. Hanger, W. Noble, Calpain cleavage and inactivation of the sodium calcium exchanger-3 occur downstream of Aβ in Alzheimer's disease, Aging Cell 13 (2014) 49–59, https://doi.org/10.1111/acel.12148.

[50] W. Noble, C. Garwood, J. Stephenson, A.M. Kinsey, D.P. Hanger, B.H. Anderton, Minocycline reduces the development of abnormal tau species in models of Alzheimer's disease, Faseb. J. 23 (2009) 739–750.

[51] A. Ferreira, Calpain dysregulation in Alzheimer's disease, ISRN Biochem 2012 (2012) 1–12, https://doi.org/10.5402/2012/728571.

[52] A. Kremer, GSK3 and Alzheimer's disease: facts and fiction…, Front. Mol. Neurosci. 4 (2011) 1–10, https://doi.org/10.3389/fnmol.2011.00017.

[53] P.T.T. Ly, J. Woodgett, W. Song, P.T.T. Ly, Y. Wu, H. Zou, R. Wang, W. Zhou, A. Kinoshita, Inhibition of GSK3 β -mediated BACE1 expression reduces Alzheimer-associated phenotypes, J. Clin. Invest. 123 (2013) 224–235, https://doi.org/10.1172/JCI64516.224.

[54] N. Jin, X. Yin, D. Yu, M. Cao, C.X. Gong, K. Iqbal, F. Ding, X. Gu, F. Liu, Truncation and activation of GSK-3β by calpain I: a molecular mechanism links to tau hyperphosphorylation in Alzheimer's disease, Sci. Rep. 5 (2015) 1–13, https://doi.org/10.1038/srep08187.

[55] P. Goñi-Oliver, J.J. Lucas, J. Avila, F. Hernández, N-terminal cleavage of GSK-3 by calpain: a new form of GSK-3 regulation, J. Biol. Chem. 282 (2007) 22406–22413, https://doi.org/10.1074/jbc.M702793200.

[56] F. Medda, B. Smith, V. Gokhale, A. Shaw, T. Dunckley, C. Hulme, Beyond secretases: kinase inhibitors for the treatment of Alzheimer's disease, Annu. Rep. Med. Chem. 48 (2013) 57–71, https://doi.org/10.1016/B978-0-12-417150-3.00005-3.

[57] C. Hooper, R. Killick, S. Lovestone, The GSK3 hypothesis of Alzheimer's disease, J. Neurochem. 104 (2008) 1433–1439, https://doi.org/10.1111/j.1471-4159.2007.05194.x.

[58] T. Kimura, K. Ishiguro, S.-I. Hisanaga, Physiological and pathological phosphorylation of tau by Cdk5, Front. Mol. Neurosci. 7 (2014) 1–10, https://doi.org/10.3389/fnmol.2014.00065.

[59] G. Šimić, M. Babić Leko, S. Wray, C. Harrington, I. Delalle, N. Jovanov-Milošević, D. Bažadona, L. Buée, R. de Silva, G. Di Giovanni, C. Wischik, P.R. Hof, Tau protein hyperphosphorylation and aggregation in alzheimer's disease and other tauopathies, and possible neuroprotective strategies, Biomolecules 6 (2016) 2–28, https://doi.org/10.3390/biom6010006.

[60] P. Theofilas, A.J. Ehrenberg, A. Nguy, J.M. Thackrey, S. Dunlop, M.B. Mejia, A.T. Alho, R.E. Paraizo Leite, R.D. Rodriguez, C.K. Suemoto, C.F. Nascimento, M. Chin, D. Medina-Cleghorn, A.M. Cuervo, M. Arkin, W.W. Seeley, B.L. Miller, R. Nitrini, C.A. Pasqualucci, W.J. Filho, U. Rueb, J. Neuhaus, H. Heinsen, L. T. Grinberg, Probing the correlation of neuronal loss, neurofibrillary tangles, and cell death markers across the Alzheimer's disease Braak stages: a quantitative study in humans, Neurobiol. Aging 61 (2018) 1–12, https://doi.org/10.1016/j.neurobiolaging.2017.09.007.

[61] L.-F. Lue, A. Guerra, D.G. Walker, Amyloid beta and tau as Alzheimer's disease blood biomarkers: promise from new technologies, Neurol Ther 6 (2017) 25–36, https://doi.org/10.1007/s40120-017-0074-8.

[62] E. Zenaro, G. Piacentino, G. Constantin, The blood-brain barrier in Alzheimer's disease, Neurobiol. Dis. 107 (2017) 41–56, https://doi.org/10.1016/j.nbd.2016.07.007.

[63] P. Preece, D.J. Virley, M. Costandi, R. Coombes, S.J. Moss, A.W. Mudge, E. Jazin, N.J. Cairns, Beta-secretase (BACE) and GSK-3 mRNA levels in Alzheimer's disease, Brain Res Mol Brain Res 116 (2003) 155–158, https://doi.org/10.1016/S0169-328X(03)00233-X.

[64] P.H. Reddy, Amyloid beta-induced glycogen synthase kinase 3β phosphorylated VDAC1 in Alzheimer's disease: implications for synaptic dysfunction and neuronal damage, Biochim. Biophys. Acta, Mol. Basis Dis. 1832 (2013) 1913–1921, https://doi.org/10.1016/j.bbadis.2013.06.012.

[65] J. Jo, D.J. Whitcomb, K.M. Olsen, T.L. Kerrigan, S.C. Lo, G. Bru-Mercier, B. Dickinson, S. Scullion, M. Sheng, G. Collingridge, K. Cho, Aβ1-42inhibition of LTP is mediated by a signaling pathway involving caspase-3, Akt1 and GSK-3β, Nat. Neurosci. 14 (2011) 545–547, https://doi.org/10.1038/nn.2785.

[66] L. Zhang, Y. Fang, Y. Xu, Y. Lian, N. Xie, T. Wu, H. Zhang, L. Sun, R. Zhang, Z. Wang, Curcumin improves amyloid β-peptide (1-42) induced spatial memory deficits through BDNF-ERK signaling pathway, PLoS One 10 (2015) 1–17, https://doi.org/10.1371/journal.pone.0131525.

[67] E. Reusche, Silver staining of senile plaques and neurofibrillary tangles in paraffin sections: a simple and effective method, Pathol. Res. Pract. 187 (1991) 1045–1049, https://doi.org/10.1016/S0344-0338(11)81084-8.

[68] J.C. Hedreen, L.S. Raskin, D.L. Price, A quick silver method for senile plaques and neurofibrillary tangles in paraffin sections, Brain Res. Bull. 35 (1994) 279–284, https://doi.org/10.1016/0361-9230(94)90135-X.

[69] C. Zussy, A. Brureau, E. Keller, S. Marchal, C. Blayo, B. Delair, G. Ixart, T. Maurice, L. Givalois, Alzheimer's disease related markers, cellular toxicity and behavioral deficits induced six weeks after oligomeric amyloid-β peptide injection in rats, PLoS One 8 (2013), https://doi.org/10.1371/journal.pone.0053117.

[70] S. Sadigh-Eteghad, B. Sabermarouf, A. Majdi, M. Talebi, M. Farhoudi, J. Mahmoudi, Amyloid-beta: a crucial factor in Alzheimer's disease, Med. Princ. Pract. 24 (2015) 1–10, https://doi.org/10.1159/000369101.

[71] Y.S. Batarseh, Q.V. Duong, Y.M. Mousa, S.B. Al Rihani, K. Elfakhri, A. Kaddoumi, Amyloid-β and astrocytes interplay in amyloid-β related disorders, Int. J. Mol. Sci. 17 (2016) 1–19, https://doi.org/10.3390/ijms17030338.

[72] F. Ul Amin, S.A. Shah, M.O. Kim, Vanillic acid attenuates Aβ1-42-induced oxidative stress and cognitive impairment in mice, Sci. Rep. 7 (2017) 1–15, https://doi.org/10.1038/srep40753.

[73] A. Currais, O. Quehenberger, A. M Armando, D. Daugherty, P. Maher, D. Schubert, Amyloid proteotoxicity initiates an inflammatory response blocked by cannabinoids, NPJ Aging Mech Dis 2 (2016) 16012, https://doi.org/10.1038/npjamd.2016.12.

[74] W. Wang, M. Tan, J. Yu, L. Tan, Role of pro-inflammatory cytokines released from microglia in Alzheimer's disease, Ann. Transl. Med. 3 (2015) 1–15, https://doi.org/10.3978/J.ISSN.2305-5839.2015.03.49.

[75] B. Kaltschmidt, C. Kaltschmidt, NF-kB in the nervous system, Cold Spring Harbor Perspect. Biol. 1 (2009) 1–14, https://doi.org/10.1101/cshperspect.a001271_erratum.

[76] F. Marques-Fernandez, L. Planells-Ferrer, R. Gozzelino, K.M.O. Galenkamp, S. Reix, N. Llecha-Cano, J. Lopez-Soriano, V.J. Yuste, R.S. Moubarak, J.X. Comella, TNFα induces survival through the FLIP-L-dependent activation of the MAPK/ERK pathway, Cell Death Dis. 4 (2013) 1–12, https://doi.org/10.1038/cddis.2013.25.

[77] G. Sabio, R.J. Davis, TNF and MAP kinase signaling pathways, Semin. Immunol. 26 (2014) 237–245.

[78] L. Planells-Ferrer, J. Urresti, E. Coccia, K.M.O. Galenkamp, I. Calleja-Yagüe, J. López-Soriano, P. Carriba, B. Barneda-Zahonero, M.F. Segura, J.X. Comella, FAIMs: more than death-receptor antagonists in the nervous system, J. Neurochem. 139 (2016) 11–21, https://doi.org/10.1111/jnc.13729.

[79] P. Carriba, S. Jimenez, V. Navarro, I. Moreno-Gonzalez, B. Barneda-Zahonero, R.S. Moubarak, J. Lopez-Soriano, A. Gutierrez, J. Vitorica, J.X. Comella, Amyloid-β reduces the expression of neuronal FAIM-L, thereby shifting the inflammatory response mediated by TNFα from neuronal protection to death, Cell Death Dis. 6 (2015), https://doi.org/10.1038/cddis.2015.6.

[80] V.M. Ho, J.-A. Lee, K.C. Martin, The cell biology of synaptic plasticity, Science 334 (2011) 623–628, https://doi.org/10.1126/science.1209236.

[81] A.R.A. Alabi, R.W. Tsien, Synaptic vesicle pools and dynamics, Cold Spring Harbor Perspect. Biol. 4 (2012) 1–18, https://doi.org/10.1101/cshperspect.a013680.

[82] S.J. Mcclure, P.J. Robinson, Dynamin, endocytosis and intracellular signalling (Review), Mol Membr Biol 13 (1996) 189–215, https://doi.org/10.3109/09687689609160598.

[83] B.L. Kelly, R. Vassar, A. Ferreira, β-amyloid-induced dynamin 1 depletion in hippocampal neurons: a potential mechanism for early cognitive decline in Alzheimer disease, J. Biol. Chem. 280 (2005) 31746–31753, https://doi.org/10.1074/jbc.M503259200.

[84] L. Pardo, L.M. Valor, A. Eraso-Pichot, A. Barco, A. Golbano, G.E. Hardingham, R. Masgrau, E. Galea, CREB regulates distinct adaptive transcriptional programs in astrocytes and neurons, Sci. Rep. 7 (2017) 1–14, https://doi.org/10.1038/s41598-017-06231-x.

[85] S. Zimbone, I. Monaco, F. Gianì, G. Pandini, A.G. Copani, M.L. Giuffrida, E. Rizzarelli, Amyloid Beta monomers regulate cyclic adenosine monophosphate response element binding protein functions by activating type-1 insulin-like growth factor receptors in neuronal cells, Aging Cell 17 (2018) 1–10, https://doi.org/10.1111/acel.12684.

[86] B. Wiedenmann, W.W. Franke, C. Kuhn, R. Moll, V.E. Gould, Synaptophysin: a marker protein for neuroendocrine cells and neoplasms, Proc. Natl. Acad. Sci. U. S. A. 83 (1986) 3500–3504, https://doi.org/10.1073/pnas.83.10.3500.
[87] T. Takeuchi, A.J. Duszkiewicz, R.G.M. Morris, The synaptic plasticity and memory hypothesis: encoding, storage and persistence, Phil. Trans. Biol. Sci. 369 (2014) 1–14, https://doi.org/10.1098/rstb.2013.0288.
[88] V. Lakhina, R.N. Arey, R. Kaletsky, A. Kauffman, G. Stein, W. Keyes, D. Xu, C.T. Murphy, Genome-wide functional analysis of CREB/long-term memory-dependent transcription reveals distinct basal and memory gene expression programs, Neuron 85 (2015) 330–345.
[89] C.D. Barnhart, D. Yang, P.J. Lein, Using the Morris water maze to assess spatial learning and memory in weanling mice, PLoS One 10 (2015) 1–16, https://doi.org/10.1371/journal.pone.0124521.
[90] S. Ghaderi, P. Gholipour, A. Komaki, I. Salehi, K. Rashidi, S. Esmaeil Khoshnam, M. Rashno, p-Coumaric acid ameliorates cognitive and non-cognitive disturbances in a rat model of Alzheimer's disease: the role of oxidative stress and inflammation, Int. Immunopharm. 112 (2022) 109295, https://doi.org/10.1016/j.intimp.2022.109295.
[91] C.V. Vorhees, M.T. Williams, Assessing spatial learning and memory in rodents, ILAR J. 55 (2014) 310–332, https://doi.org/10.1093/ilar/ilu013.
[92] J.I. Rossato, C.A. Köhler, A. Radiske, L.R.M. Bevilaqua, M. Cammarota, Inactivation of the dorsal hippocampus or the medial prefrontal cortex impairs retrieval but has differential effect on spatial memory reconsolidation, Neurobiol. Learn. Mem. 125 (2015) 146–151, https://doi.org/10.1016/j.nlm.2015.09.001.
[93] A. V Terry, Chapter 13 Spatial navigation (water maze) tasks, Methods of Behavior Analysis in Neuroscience (2009) 1–10.
[94] W.C. Leon, M.A. Bruno, S. Allard, K. Nader, A.C. Cuello, Engagement of the PFC in consolidation and recall of recent spatial memory, Learn. Mem. 17 (2010) 297–305, https://doi.org/10.1101/lm.1804410.
[95] C.D. Barnhart, D. Yang, P.J. Lein, Using the Morris water maze to assess spatial learning and memory in weanling mice, PLoS One 10 (2015) 1–16, https://doi.org/10.1371/journal.pone.0124521.
[96] P. Curzon, N.R. Rustay, K.E. Browman, Chapter 2 cued and contextual fear conditioning for rodents, in: Methods of Behavior Analysis in Neuroscience, 2009, pp. 1–11.
[97] P.J. Brasted, T.J. Bussey, E.A. Murray, S.P. Wise, Role of the hippocampal system in associative learning beyond the spatial domain, Brain 126 (2003) 1202–1223, https://doi.org/10.1093/brain/awg103.
[98] M.A. Rehbein, C. Steinberg, I. Wessing, M.C. Pastor, P. Zwitserlood, K. Keuper, M. Junghöfer, Rapid plasticity in the prefrontal cortex during affective associative learning, PLoS One 9 (2014) 1–10, https://doi.org/10.1371/journal.pone.0110720.
[99] G. Di Chen, S. Manohar, R. Salvi, Amygdala hyperactivity and tonotopic shift after salicylate exposure, Brain Res. 1485 (2012) 63–76, https://doi.org/10.1016/j.brainres.2012.03.016.
[100] O. Schmitt, P. Eipert, K. Philipp, R. Kettlitz, G. Fuellen, A. Wree, The intrinsic connectome of the rat amygdala, Front. Neural Circ. 6 (2012) 1–32, https://doi.org/10.3389/fncir.2012.00081.
[101] Z. Kiasalari, R. Heydarifard, M. Khalili, S. Afshin-Majd, T. Baluchnejadmojarad, E. Zahedi, A. Sanaierad, M. Roghani, Ellagic acid ameliorates learning and memory deficits in a rat model of Alzheimer's disease: an exploration of underlying mechanisms, Psychopharmacology (Berl) 234 (2017) 1841–1852, https://doi.org/10.1007/s00213-017-4589-6.
[102] R.C. Hider, Z.D. Liu, H.H. Khodr, Metal chelation of polyphenols, Methods Enzymol. 335 (2001) 190–203, https://doi.org/10.1016/S0076-6879(01)35243-6.
[103] D.A. Vattem, K. Shetty, Biological functionality of ellagic acid: a review, J. Food Biochem. 29 (2005) 234–266, https://doi.org/10.1111/j.1745-4514.2005.00031.x.
[104] Y.H. Choi, G.H. Yan, Ellagic Acid attenuates immunoglobulin E-mediated allergic response in mast cells, Biol. Pharm. Bull. 32 (2009) 1118–1121, https://doi.org/10.1248/bpb.32.1118.
[105] M. Sakthivel, R. Elanchezhian, E. Ramesh, M. Isai, C.N. Jesudasan, P.A. Thomas, P. Geraldine, Prevention of selenite-induced cataractogenesis in Wistar rats by the polyphenol, ellagic acid, Exp. Eye Res. 86 (2008) 251–259, https://doi.org/10.1016/j.exer.2007.10.016.
[106] S. Corbett, J. Daniel, R. Drayton, M. Field, R. Steinhardt, N. Garrett, Evaluation of the anti-inflammatory effects of ellagic acid, J. PeriAnesthesia Nurs. 25 (2010) 214–220, https://doi.org/10.1016/j.jopan.2010.05.011.
[107] L.A. BenSaad, K.H. Kim, C.C. Quah, W.R. Kim, M. Shahimi, Anti-inflammatory potential of ellagic acid, gallic acid and punicalagin A&B isolated from Punica granatum, BMC Compl. Alternative Med. 17 (2017), https://doi.org/10.1186/s12906-017-1555-0.
[108] D. Cornélio Favarin, M. Martins Teixeira, E. Lemos De Andrade, C. De Freitas Alves, J.E. Lazo Chica, C. Artério Sorgi, L.H. Faccioli, A. Paula Rogerio, Anti-inflammatory effects of ellagic acid on acute lung injury induced by acid in mice, Mediat. Inflamm. 2013 (2013) 1–13, https://doi.org/10.1155/2013/164202.
[109] Z. Wang, Neuroprotective effects of ellagic acid on neonatal hypoxic brain injury via inhibition of inflammatory mediators and down-regulation of JNK/p38 MAPK, Trop. J. Pharmaceut. Res. 15 (2016) 241–251.
[110] S. Mashhadizadeh, Y. Farbood, M. Dianat, A. Khodadadi, A. Sarkaki, Therapeutic effects of ellagic acid on memory, hippocampus electrophysiology deficits, and elevated TNF-α level in brain due to experimental traumatic brain injury, Iran J Basic Med Sci 20 (2017) 399–407, https://doi.org/10.22038/ijbms.2017.8581.
[111] T. Hajjar, Y.M. Goh, M.A. Rajion, S. Vidyadaran, T.A. Li, M. Ebrahimi, Alterations in neuronal morphology and synaptophysin expression in the rat brain as a result of changes in dietary n-6: N-3 fatty acid ratios, Lipids Health Dis. 12 (2013) 1–9, https://doi.org/10.1186/1476-511X-12-113.
[112] R.C. Malenka, Synaptic plasticity: the brain's response to experience, in: Neurosci Res, Elsevier Ireland Ltd Elsevier House, Brookvale Plaza, East Park Shannon, Co, Clare, Ireland, 2008. S1–S1.
[113] N. Bansal, P. Yadav, M. Kumar, Ellagic acid administration negated the development of streptozotocin-induced memory deficit in rats, Drug Res. 67 (2017) 425–431.
[114] J. Kaur, M. Kumar, N. Bansal, Ellagic acid administration reverses colchicine induced dementia in rats, Journal of Pharmaceutical Technology, Research and Management 4 (2016) 31–46, https://doi.org/10.15415/jptrm.2016.41003.
[115] J.P.C. De Bruin, W. a M. Swinkels, J.M. De Brabander, Response learning of rats in a Morris water maze: involvement of the medial prefrontal cortex, Behav. Brain Res. 85 (1997) 47–55, https://doi.org/10.1016/S0166-4328(96)00163-5.
[116] Y. Farbood, M. Rashno, S. Ghaderi, S.E. Khoshnam, A. Sarkaki, K. Rashidi, M. Rashno, M. Badavi, Ellagic acid protects against diabetes-associated behavioral deficits in rats: possible involved mechanisms, Life Sci. 225 (2019) 8–19, https://doi.org/10.1016/j.lfs.2019.03.078.